# Evaluation and Analysis of FBMC/OQAM Systems Based on Pulse Shaping Filters

**HEBA M. ABDEL-ATTY**[1]**, (Senior Member, IEEE), WALID A. RASLAN**[iD][2]**, (Member, IEEE), AND ABEER T. KHALIL**[3]

[1]Electrical Engineering Department, Faculty of Engineering, Port Said University, Port Said 42524, Egypt
[2]Communication and Computers Engineering Department, Faculty of Engineering, Delta University for Science and Technology, Gamasa 11152, Egypt
[3]Electrical Engineering Department, Faculty of Engineering, Benha University, Benha 13511, Egypt

Corresponding author: Walid A. Raslan (walid.raslan@ymail.com)

**ABSTRACT** Cyclic prefix orthogonal frequency division multiplexing (CP-OFDM) is the most widespread multicarrier modulation scheme. However, the use of a rectangular filter in CP-OFDM causes poor out-of-band (OoB) radiation. Moreover, the CP causes spectral efficiency loss. To overcome these limitations, a filter bank multicarrier (FBMC) was proposed which uses prototype pulse shaping filters that can be adapted to fulfil the system requirements. The choice of the filter is crucial for FBMC/offset quadrature amplitude modulation (OQAM) due to its significant impact on the achieved performance. In this paper, new prototype pulse shaping filters in FBMC/OQAM systems are proposed, aiming to improve the system performance. A number of prototype pulse shaping filters, such as raised cosine pulse (RC), root raised cosine pulse (RRC), better than raised cosine pulse (BTRC), modified Bartlett-Hanning (MBH), improved sinc power pulse (ISP), phase modified sinc pulse (PMSP), parametric linear pulse (PLP), linear combination pulse (LCP), PHYDYAS and Hermite, are considered. The performance of each pulse shaping filter in FBMC/OQAM is evaluated and compared other in terms of the power spectral density (PSD), spectral efficiency, signal-to-interference ratio (SIR), time offset (TO), carrier frequency offset (CFO) and bit error rate (BER) performance over various channels. In addition, as multiple input multiple output (MIMO) is one of the main challenges associated with FBMC, we propose the new approach that use the frequency/time block spreading based on a Walsh-Hadamard (WH) code in MIMO FBMC/OQAM and investigate the combination of the our proposed prototype pulse shaping filters with MIMO systems. The proposed filters are shown to be suitable candidates for FBMC/OQAM systems.

**INDEX TERMS** FBMC/OQAM, CP-OFDM, prototype pulse shaping filter, RC, RRC, RRC, BTRC, MBH, ISP, PMSP, PLP, LCP, PHYDYAS, Hermite, MIMO, Walsh-Hadamard.

## I. INTRODUCTION

Next-generation mobile communication systems necessitate the improvement of wireless systems to meet the new requirements in next network scenarios such as ultra-reliable and low latency communications (URLLC), enhanced mobile broadband (eMBB) and massive machine-type communications (mMTC) [1]. So that the multicarrier modulation (MCM) has been widely used; with its appealing characteristics, MCM represents the key element in wireless networks [2]. A common MCM technique is OFDM, which uses a rectangular pulse shape, and this technique is popularly used in wireless

broadband systems. OFDM has significant limitations, such as high OoB emissions, which causes interfering between the neighboring channels, CP overhead, which causes a reduction in spectral efficiency, and orthogonality, which requires stringent time and frequency synchronization to avoid frequency and timing offsets, that make it not the most suitable waveform for all targeted application scenarios [3], [4].

Many works have shown that this problem can be overcome by using new waveform designs. The waveform design is very important because everything in wireless communications systems is related to the design; thus, it is considered the heart of the wireless communication networks and is associated with the requirements of the systems and channel environment. The waveform defines what, where

The associate editor coordinating the review of this manuscript and approving it for publication was Zhen Gao[iD].

and how to transmit. The devolvement in wireless systems requires rethinking of waveforms with better characteristics, such as lower latency, complexity, power, and asynchronous, more bands, and higher security, to meet new requirements [5], [6]. To overcome the drawbacks in OFDM, FBMC was introduced [7]–[13] as one of the new waveforms. FBMC exploits the PF for each subcarrier to separate between sub-channels in the frequency domain, in which this PF differs from the rectangular pulse that is used in OFDM [13], to reduce inter-carrier interference (ICI) and OoB radiation [11]. As a result of its excellent characteristics, FBMC has served a critical position in several current and future global projects [14]–[19].

FBMC can be implemented using different schemes. In our study, we use Saltzberg's approach namely FBMC/OQAM or OFDM/OQAM. In this scheme, the orthogonality is only served in the real domain which leads to relaxing the orthogonality conditions, since this condition should be satisfied in the complex domain in OFDM. Therefore, one of the features of FBMC/OQAM seems to be that the demodulated transmitted data symbols are followed by interference triggered by the adjacent transmitted symbol in the time-frequency field [20]. The existence of this interference is a concern for some MIMO systems.

In FBMC/OQAM techniques, the transmultiplexer (TMUX) structure is used as a main element of the system. The synthesis filter bank (SFB) includes the transmitting filters, while the analysis filter bank (AFB) comprises of the corresponding receiving filters [20]. TMUX design focuses primarily on the design of the PF, as all subchannel filters are produced from this PF. The PF defines how the symbols are correlated with the dispersive channel robustness of the system. This problem leads to the design of PFs in time-selective and frequency-selective channels that are appropriate for communications. The PF has a significant impact on the time and frequency interference between data symbols (ICI and inter-symbol interference (ISI)). Hence, PF design is the pivotal issue for FBMC [20]–[23].

Since FBMC is introduced to be the alternative waveform to OFDM, in [24], FBMC performance evaluation and comparison with OFDM-based systems showed that MIMO and channel estimation, two of the primary FBMC-related problems, can be addressed. In [25], three main challenges, which face FBMC, were identified, as the orthogonality in time-variant channels, the packet overhead issue and the implementation of transmitter and receiver.

Despite the benefits compared to OFDM, to make FBMC a feasible candidate in next-generation mobile communication systems, some open problems must be solved. Generally, FBMC provides higher spectral properties than OFDM due to PF and the elimination of the CP [2], [25].

The authors in [13] showed that FBMC could be a more effective solution. A new FBMC approach to avoid interference was suggested in [2]. This system was also studied in [24], named FS-FBMC frequency spreading for multicarrier transmission. In [26], fast convolution based on a highly

tunable multi-rate filter bank scheme was proposed. Among the many techniques introduced to implement the FBMC system, the IFFT technique is the most effective. Therefore, we investigate this technique in our paper.

As the main element of the FBMC/OQAM scheme, the PF significantly impacts in two features that Influence on the performance of the system [27]. First, the PF's PSD determines the PSD of the FBMC/OQAM transmitted signal, thereby affecting the system's OoB emission efficiency [28], [29]. Second, the PF determines the FBMC/OQAM system's intrinsic interference. Since the intrinsic interference affects in the channel estimation, the PF impacts the system's channel estimation efficiency [21], [30]. Since low OoB emissions are effective in attaining a improving spectral properties and precise channel estimation [31], the design of PFs is essential to achieving the high performance required for the FBMC/OQAM scheme [32].

Since the prototype pulse shaping filter has an important effect on wireless communication system efficiency. Many works in the literature studied the effects of different pulse shaping filters on performance. In [33]–[35], the pulse shaping for reducing the ICI in OFDM has been proposed using pulses such as RC, BTRC, SP, and ISP. New pulse shapes, namely, improved PMSP, were introduced to reduce ICI OFDM in [36].

The PF design, that uses the frequency sampling method, was introduced in [20], [37]. A benefit of the selected technique is that a closed-form representation can express near-perfect reconstruction characteristics. Then, in [38], the PHYDYAS pulse shape was introduced in the EU FP7 Project. In [39], raised cosine windowed OFDM (RC-OFDM) in the CR context and PHYDYAS and the isotropic orthogonal transform algorithm (IOTA) for OQAM were evaluated for their performance. Furthermore, BTRC, which is used to improve the ICI in OFDM, was proposed and the OoB reduction and ICI power reduction were addressed in [40]. In [41], different window functions were used to study the BER performance due to each of the pulse shapes.

A comparative study of FBMC PFs was provided in [42]. Rectangular, extended rectangular, RRC, optimal finite duration pulse, Hermite, PHYDYAS, and IOTA filters were considered. The Hermite and IOTA filters eliminated CP use, achieved a greater SIR for higher frequency dispersion, and offered lower sidelobe. The PHYDYAS PF attained the best SIR performance that enabled less complicated reception and transmitter structures.

The authors in [43], [44] investigated the IOTA filter in OFDM, but the drawback of this method is the intrinsic interference. Based on a comparison of PHYDYAS with IOTA in the FBMC system, PHYDYAS presented a better performance [45]. Various schemes to reduce the peak-to-average power ratio (PAPR) and ICI have been introduced in the literature. These schemes consist of the improved modified Bartlett–Hanning pulse [46], [47] and the improved parametric linear combination pulse (IPLCP) [48], [49], to improve the OFDM system error performance and reduce the ICI.

The efficiency of IPLCP was analysed in multiplexing schemes based on OFDM in [50], [51]. Additionally, the sinc parametric linear combination pulse (SPLCP) was proposed in [52] and the PMSP was proposed in [53] which attempts to reduce the amplitude of the sidelobes and leads to much better BER performance than ISP. Many pulse shaping filters, such as the exponential linear pulse, were proposed in [54], [55] to decrease the ISI impact in the OFDM scheme. Furthermore, many of these Nyquist pulse shaping filters were used to reduce the sensitivity to symbol timing error in generalized frequency division multiplexing (GFDM) such as in [56]–[58].

In FBMC systems, the prototype pulse shaping filter has been suggested to reduce OoB emission. Many literature works [2], [20], [23], [27], [59]–[61] focused on the design of pulse shaping filters for FBMC with the aim of reduction of OoB emission. In [59], OFDM and orthogonal Hermite signals were compared by measuring their time-bandwidth products (TBP). In [2], the PHYDYAS filter was employed in FFT/IFFT-based convolution FBMC/OQAM. In [60], PHYDYAS and Hermite filters were considered to evaluate the performance of FBMC/OQAM.

In this paper, we propose different pulse shaping filters, such as BTRC, MBH, ISP, PMSP, PLP, and LCP, in the design of a PF for the FBMC/OQAM system. The ability of these proposed pulse shaping filters to improve MCM in OFDM has been proven, as mentioned in the literature. Furthermore, a comparison between the proposed pulses and some well-known pulse shaping filters, such as RC, RRC, PHYDYAS, and Hermite, is provided.

Another problem that comes when developing an FBMC scheme is its compatibility with MIMO. Since MIMO FBMC/OQAM is a really interesting possible technique for the next generation of wireless communications systems. Indeed, applying OFDM to MIMO channels is a simple statement, but the direct deployment of FBMC to MIMO channels is a non-trivial issue due to the intrinsic interference and omitted CP [62]. While the PF is the key to the FBMC/OQAM communication system, choosing well-localized filters in the time and frequency domains is desirable to enhance MIMO FBMC/OQAM [63]. Recently, the use of FBMC/OQAM transmission has been extended to both MIMO and massive MIMO systems [64].

Several studies on different FBMC schemes have recently been carried out. The authors in [65], [66] investigated the combination of OFDM/OQAM using the IOTA function and MIMO over radio channels Pedestrian A and Vehicular A and showed that spatial multiplexing (SM) MIMO could be directly applied to OFDM/OQAM. The space-time block coding (STBC) Alamouti code together with OFDM/OQAM was not included in their work. Regarding the Alamouti scheme, its straightforward application to FBMC generates an intrinsic interference which cannot be simply overcome [67], [68]. There have been several works on this subject, such as [67], Whereby the authors found that Alamouti coding may be executed only when it has come with code division

multiple access (CDMA), considering the two different pulse shapes IOTA and PHYDYAS. However, this method is very sensitive to time variations of the channel and requires high computational complexity. The pseudo-Alamouti system was proposed in [69] at the cost of spectral efficiency as it needs a CP to be inserted to the FBMC signal.

Blockwise Alamouti systems were provided for the FBMC using the PHYDYAS PF [70], [71]. In these arrangements, the transmitted symbols were coded in a time or frequency inversion frame structure. Hence, traditional Alamouti decoding could be used after FBMC demodulation to decoding the received symbols. These systems are simple to deploy and do not damage the FBMC data structure. However, serious degradation occurs in high-frequency selective channels because the channel frequency response should be flat on each subcarrier to maintain full diversity in the receiver.

While FBMC/OQAM constructs the orthogonality in the real field with imaginary interference which causes the intrinsic imaginary interference [72]. This increases the complexity of the analytical description of detection in MIMO systems. Recent work in [68] investigates symbol-error-rate (SER) of the FBMC-OQAM based MIMO systems for the MMSE detection. Also, the channel and CFO effects have been considered in [73]. In [74], a new technique is investigated for the detection in MIMO-FBMC-OQAM systems called neighborhood detection based ZF-successive interference cancellation (ND-ZF-SIC).

The authors in [75], [76] introduced a very effective solution to recover complex orthogonality in FBMC by spreading data symbols in frequency or time. These techniques enable to apply of all MIMO methods that may be used in OFDM to FBMC. The spreading technique itself has not added more complexity since it depends on a fast Walsh-Hadamard (WH) transformation which is considered the multiplication-free scheme. The FBMC/OQAM system studied in these works [75], [76] was evaluated based on the PHYDYAS PF in the case of frequency spreading [75] and the Hermite PF in the case of time spreading.

From the work performed by various researchers on the FBMC in the literature, various observations can be drawn: i) FFT-FBMC implementation is the most efficient technique. ii) PF design is the primary issue affecting all parameters for FBMC. iii) To our knowledge, no study has yet addressed the employed of the FBMC PF design with the Nyquist pulse shaping filters such as BTRC, MBH, ISP, PMSP, PLP, and LCP. However, when used in GFDM and OFDM, as shown in the literature, these pulse shaping filters achieve better efficiency. iv) MIMO compatibility is one of the biggest challenges for FBMC.

In this paper, we propose the new pulse shaping filters that can be used in FBMC/OQAM systems and study their characteristics. Furthermore, we analyse and compare the performance of FBMC/OQAM over various channels using the proposed pulse shaping filters in terms of the PSD, spectral efficiency, SIR, TO, CFO and BER performance.
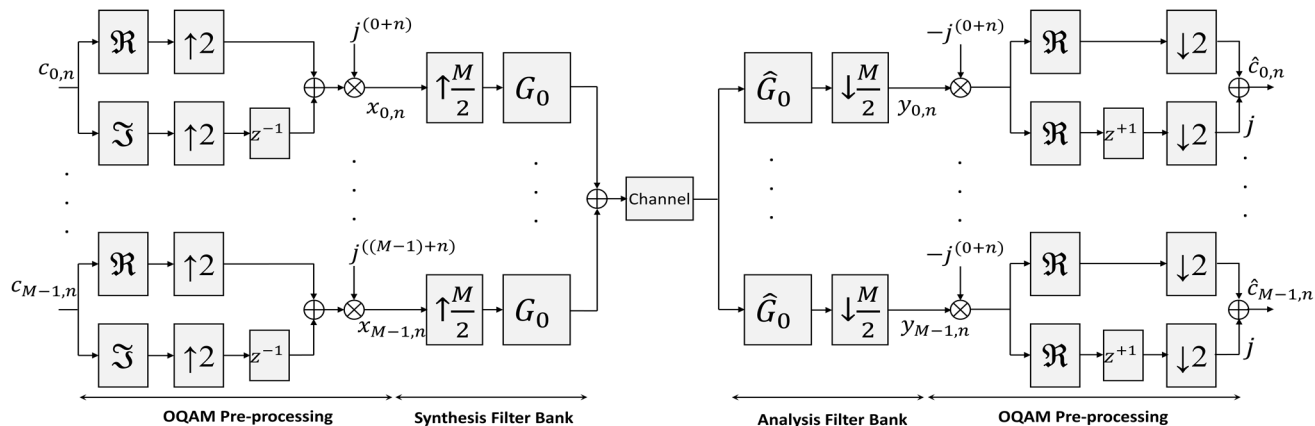
**FIGURE 1.** The TMUX scheme for FBMC/OQAM transceiver [20].

Additionally, we employ WH spreading [75], [76] to propose a new MIMO FBMC/OQAM approach using the proposed pulse shaping filters, evaluate the performance of these approaches with well-known MIMO schemes and compare them with PHYDYAS, Hermite in FBMC and CP-OFDM.

We summarize the main contributions of this paper as follows:

1) New prototype pulse shape filters are proposed to improve the performance of FBMC/OQAM systems.
2) The PLP and LCP filters may be considered promising PFs for FBMC/OQAM.
3) The WH spreading approaches allow applying the MIMO schemes that were used in OFDM, to FBMC/OQAM.

The rest of this paper is organized as follows. In section II, the standard FBMC/OQAM system model is reviewed, with an illustration of the transmitter and receiver process, and both MIMO SM and STBC Alamouti schemes combined with FBMC/OQAM are introduced. Furthermore, the matrix representation for FBMC/OQAM is described. The proposed pulse shaping filters and block spreading for FBMC/OQAM are given in section III. In section IV, the performance of the proposed schemes under various practical channels is provided via simulation results. Finally, the paper is concluded in section V.

## II. FBMC/OQAM SYSTEM MODEL

In FBMC/OQAM, let $x_{m,n}$ is the complex transmitted symbol at $m$ subcarrier and $n$ time. Then, each subcarrier shape using well-localization transmitted PF $g_{m,n}(t)$ and, finally, the transmitted signal s(t) can be expressed as [60].

$$s(t) = \sum_{n=1}^{N} \sum_{m=1}^{M} g_{m,n}(t) x_{m,n}(t) \qquad (1)$$

$$g_{m,n}(t) = p_{tx}(t - NT_0/2) e^{j2\pi mF(t - NT0)} e^{j\theta_{m,n}} \qquad (2)$$

where $p_{tx}(t)$ is the basic pulse shaping PF and $g_{m,n}(t)$ represent the shifted frequency and time version of the basic PF with $T_0$ indicate to the time spacing, $F$ is the subcarrier

spacing, $N$ is the total number of symbols and $M$ is the total number of subcarriers. At the receiver side, the received symbols can be obtained by projection of the $r(t)$ (receiving signal) and received PF.

$$y_{m,n}(t) = \langle r(t), q_{m,n}(t) \rangle = \int_{-\infty}^{\infty} r(t) q_{m,n}^*(t) dt \qquad (3)$$

where $q_{m,n}(t)$, is similarly defined as $g_{m,n}(t)$, except that a different PF might be used:

$$q_{m,n}(t) = p_{rx}(t - NT_0/2) e^{j2\pi mF(t - NT0)} e^{j\theta_{m,n}} \qquad (4)$$

The received PF $q_{m,n}(t)$ can be described as a transmitted one. In case of an Additive White Gaussian Noise (AWGN) channel, $q_{m,n}(t) = g_{m,n}(t)$. However, $q_{m,n}(t)$ may differ from $g_{m,n}(t)$ in a selective fading channel.

FBMC was introduced in [27], is namely FBMC/OQAM or staggered modulated multitoned (SMT), use the OQAM instead of QAM which the real and imaginary components are staggered by $T_0/2$. This scheme is promising techniques which can relax the orthogonality condition for real symbol only. Also, it has better spectral efficiency than OFDM while it doesn't need CP insertion [77].

Fig. 1 shows the TMUX structure of the FBMC/OQAM system [20]. In TMUX, the PF is the primary element in the scheme since all filters are obtained from this PF. As shown in Fig. 1, the transmitter includes two main processes which are OQAM pre-processing, SFB since the receiver main processes are AFB and OQAM post-processing. A delay $z^{-D}$ is added to the output of SFB and input of AFB to adjust the phase for the downsampling process. Where D relies on the PF length $L_p$ [27].

$$L_p = KM + 1 - D \qquad (5)$$

For filter length $L_p = KM - 1$, the value of $D$ will be 2 and delay $z^{-2}$. Where K is the overlapping factor.

### A. FBMC/OQAM TRANSMITTER
The OQAM pre-processing convert the complex input symbol $c_{m,n}$ to real symbol [2]. Then, the real and imaginary

components of $c_{m,n}$ are upsampled by 2.

$$c_{m,n}^R = \begin{cases} \Re\{c_{m,n/2}\} & n \quad even \\ 0 & elsewhere \end{cases} \tag{6}$$

$$c_{m,n}^I = \begin{cases} \Im\{c_{m,n/2}\} & n \quad even \\ 0 & elsewhere \end{cases} \tag{7}$$

The transmitted symbol $x_{m,n}$ is the combination of real and imaginary components.

$$x_{m,n} = x_{m,n}^R + x_{m,n}^I \tag{8}$$

In the SFB, the $x_{m,n}$ is upsampled by factor $M/2$. The filtration process is applied to each subcarrier using a shifted version of the PF $g_m[k]$ to obtain the transmitted signal. As in (1), we can express the discrete transmitted signal s[k] as [78], [79]:

$$s[k] = \sum_{n=-\infty}^{+\infty} \sum_{m=0}^{M-1} x_{m,n} g_m[k - nM/2], \tag{9}$$

and,

$$g_m[k] = e^{j\frac{2\pi}{M}mk} g[k] \tag{10}$$

### B. FBMC/OQAM RECEIVER
In the AFB, the demodulated symbol $y_{m,n}$ can be obtained by the projection of the received signal $r[k]$ on the corresponding receive filter $\hat{g}_m[k]$ as (3)

$$y_{m,n} \triangleq \sum_{k=-\infty}^{+\infty} r[k]\hat{g}_m[k - nM/2], \tag{11}$$

where

$$\hat{g}_m[k] = g_m^*[k] = e^{-j\frac{2\pi}{M}mk} g[k] \tag{12}$$

Then, the received signal will be

$$y_{m,n} = x_{m,n} + ju_{m,n} \tag{13}$$

where $u_{m,n}$ is the *intrinsic interference*, is the imaginary interference and is described as [2].

$$u_{m,n} = \sum_{(\bar{m},\bar{n})\neq(m,n)} x_{\bar{m},\bar{n}} \underbrace{g_{\bar{m}}[k - \bar{n}M/2]\hat{g}_m[k - nM/2]}_{\langle p \rangle_{\bar{m},\bar{n}}^{m,n}} \tag{14}$$

The TMUX response, $\langle p \rangle_{\bar{m},\bar{n}}^{m,n}$, depend on the PF. Then, the complex received symbol $\hat{c}_{m,n}$ cab be obtained from $y_{m,n}$ in the OQAM post-processing as in Fig. 1.

### C. MATRIX-BASED SYSTEM MODEL
In this subsection, we represent the system model in Matrix form for simplicity [60]. The transmitted PF can be defined by $G \in \mathbb{C}^{1 \times MN}$ matrix.

$$G = [g_{1,1} \cdots g_{M,1} g_{1,2} \cdots g_{M,N}] \tag{15}$$

and transmitted symbols $x \in \mathbb{C}^{MN \times 1}$, are described as:

$$x = [x_{1,1} \ x_{2,1} \ \ldots \ x_{M,1} \quad x_{1,2} \ \ldots \ x_{M,N}]^T \tag{16}$$

We can rewrite transmitted signal s(t) that is given in (1)

$$s = Gx \tag{17}$$

Similar as in (15), the sampled receive basis pulses $q_{m,n} \in \mathbb{C}^{1 \times MN}$, can also be stacked in a matrix according to [60].

$$Q = [q_{1,1} \cdots q_{M,1} q_{1,2} \cdots q_{M,N}] \tag{18}$$

If AWGN is assumed, that is, $Q = G$. In the fading channels, the $h[m_\tau, n]$ is the time-variant impulse response, and $m_\tau$ is the channel delay [80]. The channel convolution matrix can be expressed as:

$$[H]_{i,j} = h[i - j, i] \tag{19}$$

As in (3), the received symbols can be reformulated by

$$y = Q^H r = Q^H HGx + n \tag{20}$$

where $r \in \mathbb{C}^{N \times 1}$ represents the received signal and $n \sim \mathcal{CN}(0, P_n Q^H Q)$ is the Gaussian distribution noise, with $P_n$ the time white Gaussian noise power. We can neglect the channel interference because, in the highly underspreading channels, the interference is smaller than noise. Thereby, this leads to neglect of all elements of $Q^H HG$ matrix except for the diagonal elements. Then, equation (20) can be rewritten as [60]:

$$y \approx diag\{h\} Q^H Gx + n \tag{21}$$

Since FBMC/OQAM keep only orthogonality in real, this leads to $\Re\{Q^H G\} = \Re\{G^H G\} = I_{NK}$. The imaginary interference can be eliminated by phase equalizing and take real only. It will be described in more detail in MIMO.

### D. FBMC/OQAM WITH MIMO SYSTEMS
MIMO allows the wireless system to use multiple antennas which allows to increase data rate and /or more robustness. This subsection aims to give the basics of FBMC/OQAM with MIMO systems, both MIMO SM and STBC Alamuoti schemes in combination with FBMC/OQAM are considered. Then, in section III, we describe the block spread FBMC/OQAM system. Furthermore, we describe the optimal spreading matrix and explain why WH spreading is a more practical solution. Then, we discuss two possible spreading approaches in FBMC/OQAM and evaluate its performance in section IV.

In case of a single antenna, if $x_{m,n}^j$ is the transmitted symbol, then the demodulated signal $y_{m,n}^i$ is given by [67], [79]:

$$y_{m,n}^i \approx h_{m,n}^{ij}(x_{m,n}^j + ju_{m,n}^j) + \eta_{m,n}^i \tag{22}$$

where $j$ is the index for transmitted antenna and $i$ for the received antenna. $h_{m,n}^{ij}$ presents the channel and $\eta_{m,n}^i$ is the noise part at the receiving antenna $i$. $u_{m,n}^j$ is the intrinsic interference as in (13).

Therefore, when using $N_t$ antennas to transmit $N_t$ data symbols and using $N_r$ antennas to receive the transmitted

signals in the MIMO system, the FBMC demodulated signal at the receiving antenna $i$ is described by [67]:

$$y_{m,n}^{(i)} = \sum_{i=1}^{N_t} h_{m,n}^{ij}(x_{m,n}^i + ju_{m,n}^j) + \eta_{m,n}^j \qquad (23)$$

Then, the received signal matrix can be described as:

$$\begin{bmatrix} y_{m,n}^1 \\ \vdots \\ y_{m,n}^{N_r} \end{bmatrix} = \underbrace{\begin{bmatrix} h_{m,n}^{11} & \cdots & h_{m,n}^{1N_t} \\ \vdots & \ddots & \vdots \\ h_{m,n}^{N_r 1} & \cdots & h_{m,n}^{N_t N_r} \end{bmatrix}}_{H_{m,n}} \underbrace{\begin{bmatrix} x_{m,n}^1 + ju_{m,n}^1 \\ \vdots \\ x_{m,n}^{N_t} + ju_{m,n}^{N_t} \end{bmatrix}}_{x_{m,n}+ju_{m,n}} + \underbrace{\begin{bmatrix} \eta_{m,n}^1 \\ \vdots \\ \eta_{m,n}^{N_r} \end{bmatrix}}_{\eta_{m,n}}$$

$$(24)$$

$$y_{m,n} = H_{m,n}(x_{m,n}+ju_{m,n}) + \eta_{m,n} \qquad (25)$$

where $H_{m,n}$ represents the $(N_r \times N_t)$ channel matrix.

### 1) STBC ALAMOUTI SCHEMES

Applying Alamouti schemes to the FBMC/OQAM in a straightforward way makes an intrinsic interference appear, relying on the complex orthogonal system, unlike the FBMC system only has real orthogonality. Using WH CDMA coding allows holding complex orthogonality in FBMC/OQAM.

Let $x_1$ and $x_2$ be two symbols in the frequency-time grid, simultaneously transmit from antenna 1 and 2, respectively. Thereafter, in the following time slot, the $-\overleftarrow{x}_2^*$ is transmitted from antenna 1 and $\overleftarrow{x}_1^*$ from antenna 2. where $-\overleftarrow{x}_2^*, \overleftarrow{x}_1^*$ are the reversed time of $x_2, x_1$, respectively [71]. If the channels are the time-invariant throughout the transmitting time of two-time slots. The two receiving antennas collect the two signal as the following:

$$y_1 = h_1 T_0 \otimes x_1 + h_2 T_0 \otimes x_2 + n_1 \qquad (26)$$

$$y_2 = h_2 T_0 \otimes \overleftarrow{x}_1^* - h_2 T_0 \otimes \overleftarrow{x}_2^* + n_2 \qquad (27)$$

$$\overleftarrow{y}_2^* = h_2^* \overleftarrow{T}_0^* \otimes x_1 - h_1^* \overleftarrow{T}_0^* \otimes x_2 + \overleftarrow{n}_2^*$$
$$= h_2^* T_0 \otimes x_1 - h_1^* T_0 \otimes x_2 + \overleftarrow{n}_2^* \qquad (28)$$

where $\otimes$ is the convolution operator, and $n_1$ is the noise.

The last level of equality is due to the reality that $T_0$ is conjugate symmetrical along the time axis $(\overleftarrow{T}_0 = T_0)$. Therefore, we have to apply the decoding of Alamouti. We can write it [67]:

$$\bar{y}_1 = \frac{h_1^* y_1 + h_2 \overleftarrow{y}_2^*}{|h_1|^2 + |h_2|^2} = T \otimes x_1 + \frac{h_1^* n_1 + h_2 \overleftarrow{n}_2^*}{|h_1|^2 + |h_2|^2} \qquad (29)$$

$$\bar{y}_2 = \frac{h_2^* y_1 + h_1 \overleftarrow{y}_2^*}{|h_1|^2 + |h_2|^2} = T \otimes x_2 + \frac{h_2^* n_1 - h_1 \overleftarrow{n}_2^*}{|h_1|^2 + |h_2|^2} \qquad (30)$$

$$T_0 \otimes x = x + u \qquad (31)$$

The transmitted symbols can be obtained by taking real part or imaginary part of $x$ since the interference part $u$ is pure imaginary when a symbol is pure real and vice versa.

### 2) SPATIAL MULTIPLEXING (SM) WITH ZERO FORCING (ZF) DETECTION

In FBMC/OQAM, applying the linear equalizer, such as ZF with SM schemes, can be implemented as in [65] since virtual transmitted symbols $a_{mn}$. Linear equalizer as ZF in SM system in FBMC/OQAM scheme can be performed as described in [65] where a virtually transmitted vector $a_{m,n}$ is regarded as well as the real symbols and described as:

$$a_{m,n} = x_{m,n} + ju_{m,n} \qquad (32)$$

The equalized virtual symbols $\tilde{a}_{m,n}$ can be expressed as:

$$\tilde{a}_{m,n} = G_{m,n}^H r_{m,n} \qquad (33)$$

where $r_{m,n}$ is the received symbols and $G_{m,n}$ is the matrix of equalization based on ZF. The real part retrieval of $\tilde{c}_{m,n}$ then produces the real equalized vector $\tilde{x}_{m,n}$ [65].

### 3) SPATIAL MULTIPLEXING (SM) WITH MAXIMUM LIKELIHOOD (ML) DETECTION

The ML detection is the best in that it minimizes the likelihood of error [81]. Indeed, the existence of the interference vector $U_{m,n}$ expression in (31) blocks the applying of ML individually at each time-frequency grid $(m,n)$ because the interference has a large effect and depends on the neighbor symbol.

In the ML system, all transmitted symbols in the frame take into consideration. Let's consider a multicarrier symbol data $x$. Then, $x$ contains $(M \times N)$ components and each $x_{m,n}$ component is a real vector of $(N_t \times 1)$. On the receiver side, we also get a $(M \times N)$ frame $r$ whose $r_{m,n}$ elements are complex vectors $(N_r \times 1)$. The ML technique involves detecting the frame $x$ between all possible frames which make the receiving probability of the frame $r$ is maximum when $x$ frame is transmitted [80], the detected signal can be written as:

$$y = \underset{x}{\arg\max} \{P(r/x)\} \qquad (34)$$

## III. PROPOSED APPROACHES

In this section, we propose two approaches which are two significant issues in FBMC/OQAM. Firstly, we propose some pulse shaping filters such as BTRC, MBH, ISP, PMSP, PLP, and LCP to improve the performance of the FBMC waveform. Furthermore, we investigate some PFs, which have been mentioned in the literature, such as RC, RRC, PHY-DYAS, and Hermite in our work to compare with proposed filters. Also, we provide the description of their mathematical representation and main parameters that affect the impulse and frequency response of these pulses which is reflected on the whole FBMC properties. As we described that a prototype pulse shaping filters have a great impact on the FBMC spectral properties. Secondly, we propose an effective promising scheme that can restore complex orthogonality in FBMC/OQAM which enables to combine the MIMO with FBMC with low complexity.
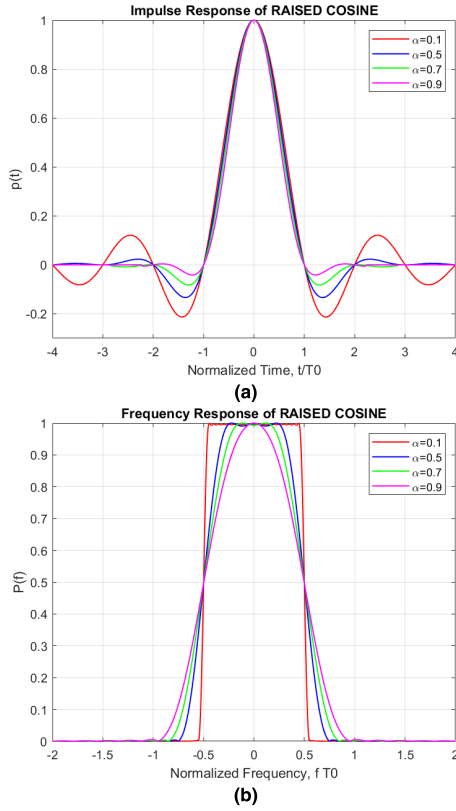
**FIGURE 2.** (a) Impulse and (b) frequency response of RC.



**FIGURE 3.** (a) Impulse and (b) frequency response of RRC.

### A. PROTOTYPE PULSE SHAPING FILTERS

#### 1) RAISED COSINE (RC) FILTER

The RC filter is the pulse shaping filter used to minimize the ISI. The impulse response of this filter as given in [82] is given by:

$$p_{RC} = \sin c\left(\frac{t}{T_0}\right)\frac{\cos(2\pi\alpha t)}{1-(2\alpha t/T_0)^2} \quad (35)$$

In this pulse shaping filter, $\alpha$ is the roll-off factor. The asymptotic decay rate of this pulse shaping filter is $t^3$. The RC impulse and frequency response for $\alpha$ equal to 0.1, 0.5, 0.7 and 0.9 are shown in Fig. 2.

#### 2) ROOT RAISED COSINE (RRC) FILTER

In digital communication, RRC is mostly used as a transmitting and receiving filter. The impulse response of RRC is given in [83].

$$p_{RRC}(t) = \frac{\sin\left[\frac{\pi t}{T_0}(1-\alpha)\right] + \left(\frac{4\alpha t}{T_0}\right)\cos\left[\frac{\pi t}{T_0}(1+\alpha)\right]}{\frac{\pi t}{T_0}\left[1-\left(\frac{4\alpha t}{T_0}\right)^2\right]} \quad (36)$$

The impulse response of this filter is not zero at intervals $\pm T$. But at $\alpha = 0$, the zeros of this filter is at $\pm T$. Fig. 3 shows the RRC filter impulse and frequency response for $\alpha$ equal to 0.1, 0.5, 0.7 and 0.9.

#### 3) BETTER THAN RAISED COSINE (BTRC) FILTER

This pulse shaping filter is given in [40], [84] and the impulse response of this filter is described as:

$$p_{BTRC}(t) = \sin c\left(\frac{t}{T_0}\right)\frac{\frac{2\beta t}{T_0}\sin\left(\frac{\pi\alpha t}{T_0}\right) + 2\cos\left(\frac{\pi\alpha t}{T_0}\right) - 1}{1 + \left(\frac{\beta t}{T_0}\right)^2} \quad (37)$$

where $\beta = \ln(2)/\alpha B$ is the bandwidth. The asymptotic decay rate of this filter is $t^2$. Fig. 4 shows the BTRC filter impulse and frequency response of for $\alpha$ equal to 0.1, 0.5, 0.7 and 0.9.

#### 4) MODIFIED BARTLETT HANNING (MBH) FILTER

This pulse shape is given in [85] and the impulse response of this pulse shape is given by:

$$p_{MBH}(t) = \sin c\left(\frac{t}{T_0}\right)$$
$$\times\left[\frac{2(1-\beta)\cos\left(\frac{\pi\alpha t}{T_0}\right)}{1-\left(\frac{2\alpha t}{T_0}\right)^2} - \frac{(1-2\beta)\sin\left(\frac{\pi\alpha t}{T_0}\right)}{\left(\frac{\pi\alpha t}{T_0}\right)}\right] \quad (38)$$

In this pulse shape, $\beta$ is the window factor which can take values between 0.5 and 1.88 [85]. Fig. 5 shows the MBH filter impulse and frequency response for $\alpha$ equal to 0.1, 0.5, 0.7 and 0.9 and $\beta$ equal 0.5, 1.2 and 1.8.

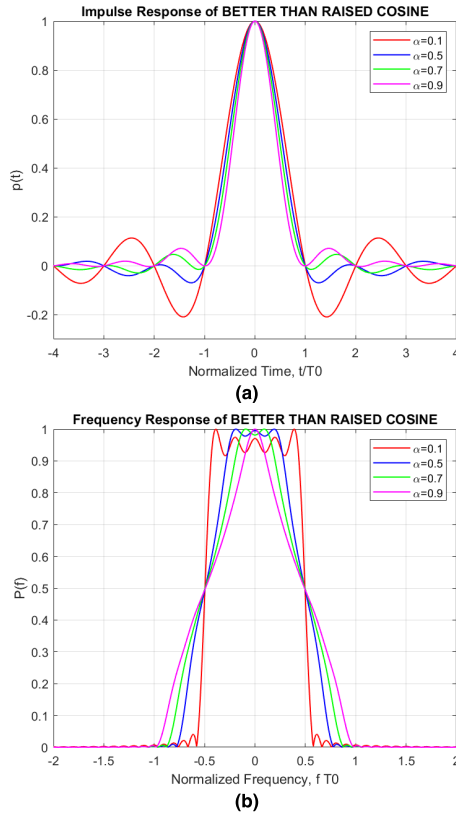**FIGURE 4.** (a) Impulse and (b) frequency response of BTRC.



**FIGURE 5.** (a) Impulse and (b) frequency response of MBH.

### 5) IMPROVED SINC POWER (ISP) SHAPING FILTER

This improved pulse is proposed in [33]. The impulse response of this improved pulse is expressed by:

$$p_{ISP}(t) = \exp\left(-a\left(\frac{t}{T_0}\right)^2\right) . \sin c^n\left(\frac{t}{T_0}\right) \qquad (39)$$

where $a$ is the designed parameter and n is the power of the sinc. Fig. 6 shows the impulse response of ISP pulse shaping filter at different values of $a$ and n. At $a = 0.5, 1, 5$ and $10$ and $n = 1$ and $2$, the ISP pulse has wider main lobe width and sidelobe width. The impulse response of this pulse shape does not depend on the roll-off factor.
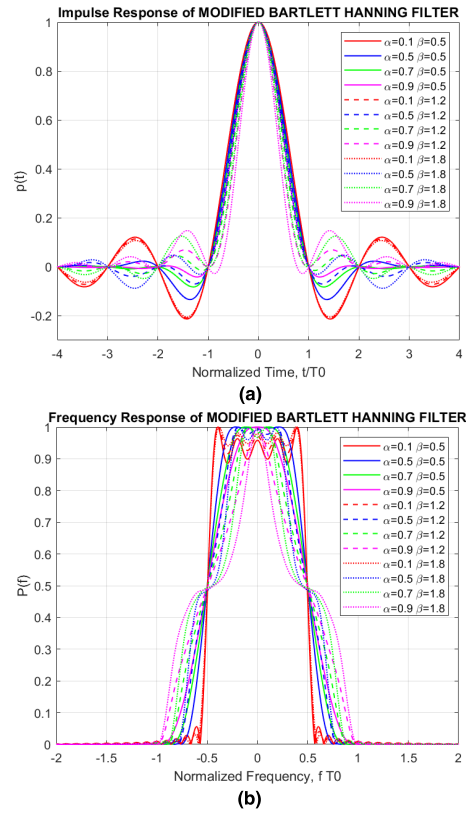
### 6) PHASE MODIFIED SINC PULSE (PMSP)

This pulse shape is proposed in [36] and the time representation of this pulse shape is given by:

$$p_{PMSP}(t) = \exp\left(-a\left(\frac{t}{T_0}\right)^2\right)\left(\frac{\sin\left((\pi t - b\sin(c\pi t))/T_0\right)}{(\pi t - b\sin(c\pi t))/T_0}\right) \qquad (40)$$

where $a$ is used for amplitude control, $b$ and $c$ are phase control parameters and $n$ is the degree of sinc function.

Fig. 7 and 8 show the impulse and frequency response of PMSP at different values of $a$, $b$ and $n$. The value of $c$ is taken as 2. At a =0.5 and n=1, the SM pulse has a wider main lobe width and sidelobe width. The impulse response of this pulse shape does not depend on the roll-off factor.

### 7) PARAMETRIC LINEAR PULSES (PLP)

A Parametric Construction of Nyquist ISI-Free Pulses family are introduced in [86], whereas the PLP filter is given by

$$p_{PLP}(t) = \sin c\left(\frac{\pi t}{T_0}\right)\sin c^n\left(\frac{\alpha\pi t}{nT_0}\right) \qquad (41)$$

The asymptotic decay rate of the PLP proportional to $1/t^n$ which has lower time jitter sensitivity than the RC pulse. Fig. 9 shows the PLP impulse and frequency response for $n$ equals 1 and 2. According to [87], [88], the amplitude of the first two sidelobes have the greatest effect on PAPR and error probability. Thus, choosing the appropriate filters based on their rate of decay is a necessity when attempting to reduce transmission errors. An important remark from the findings of [89] shows that the pulse shaping filter reducing PAPR has very low sidelobes in its time response. Hence, by selecting the proper decay rate of the filter, we are minimizing the energy contained in the tails; hence, reducing the PAPR of the system.

### 8) LINEAR COMBINATION PULSES (LCP)

The new Nyquist pulses can be produced by linearly combining of different decay rate ISI-free pulses. These pulses contain a new design parameter, defined as the linear combination constant, offering an extra degree of freedom to reduce the error throughout the case of time errors.
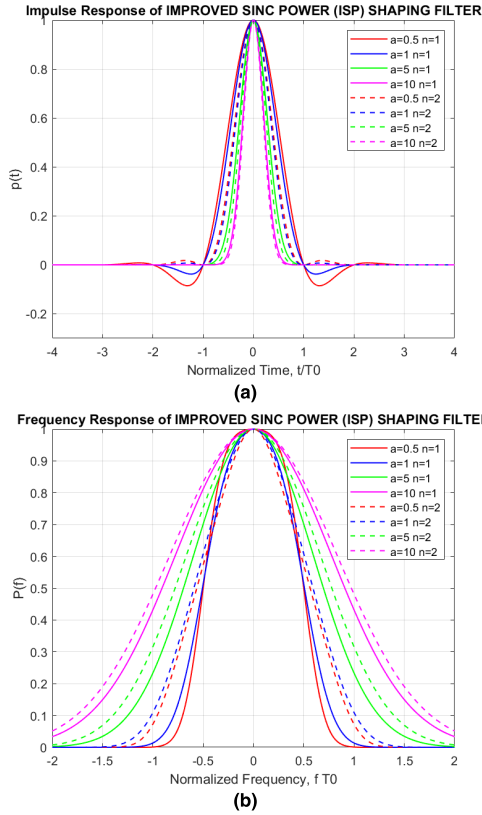
**FIGURE 6.** (a) Impulse and (b) frequency response of ISP.



**FIGURE 7.** (a) Impulse and (b) frequency response of PMSP for n = 1.

The proposed LCP pulses have more factors, $\gamma \; or \; \mu$, giving an additional degree of freedom to design a pulse with better performance. Furthermore, the bandwidth of the pulse which generating by linearly combining of two pulses that completely overlap in spectral-domain is the same as the bandwidth of the constituent pulses. Also, if the combing pulses are ISI-free, then, the combining pulse will achieve the Nyquist-I criterion [89].

*Linear Combination Pulse (LCP):* The LCP is resulting from the linearly combining of the RC pulse with the PLP pulse ($n = 1$), and the time-representation of this pulse can be defined by

$$p_{LCP}(t) = \gamma p_{PLP_{n=1}}(t) + (1 - \gamma)p_{RC}(t) \qquad (42)$$

Then, by applying (35) and (41) in (42), the LCP can be given by

$$p_{LCP}(t) = \sin c \left( \frac{\pi t}{T_0} \right)$$

$$\times \left( \gamma \sin c \left( \frac{\pi \alpha t}{T_0} \right) + \frac{(1 - \gamma) \cos \left( \frac{\pi \alpha t}{T_0} \right)}{1 - \left( \frac{\alpha t}{T_0} \right)^2} \right) (43)$$

The parameter $\gamma$ represents the combination constant which is chosen to reduce the corresponding amplitude of the biggest sidelobes and decrease the OoB emissions [86].
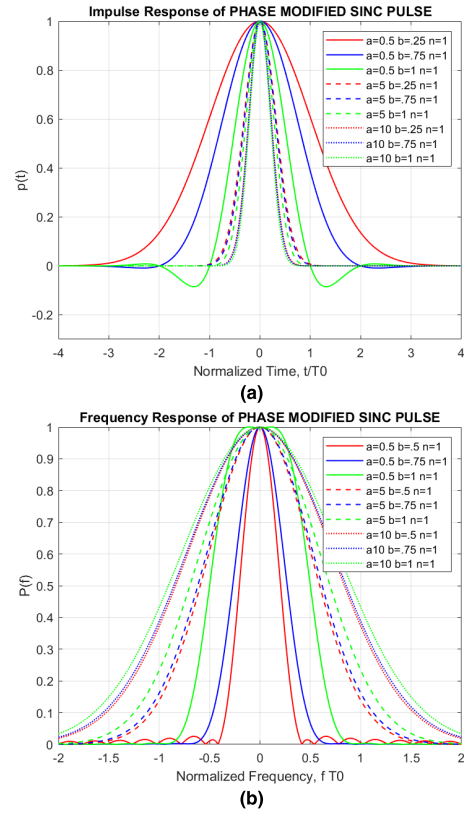
As shown in Fig. 10, the LCP achieve the Nyquist-I criterion, where the zero inter-symbol situation maintains

*Parametric Linear combination pulses (PLCP):* The PLCP is the second linear combination pulse that is resulting from combining the two PLP pulse with a different degree. As the LCP, the combining parameter, $\mu$, add an additional degree of freedom which can reduce the errors due to the symbol time error. Since the two PLP pulse are the ISI-free pulses, the PLCP will be ISI-free and can be given by

$$p_{PLCP}(t) = \mu p_{PLP_{n=1}}(t) + (1 - \mu)p_{PLP_{n=2}}(t) \qquad (44)$$

The impulse responses of $PLP_{n=1}$ and $PLP_{n=2}$ were given in (41), respectively. The impulse response of the $PLP_{n=1}$ pulse decays as $1/t^2$, while the $PLP_{n=2}$ pulse decays as $1/t^3$ [86]. Thereby, the PLCP is defined as

$$p_{PLCP}(t) = \sin c \left( \frac{\pi t}{T_0} \right)$$

$$\times \frac{4(1 - \mu) \sin^2 \left( \frac{\pi \alpha t}{2T_0} \right) + \frac{\pi \alpha \mu t}{T_0} \sin \left( \frac{\pi \alpha t}{T_0} \right)}{\left( \frac{\pi \alpha t}{T_0} \right)^2} \quad (45)$$

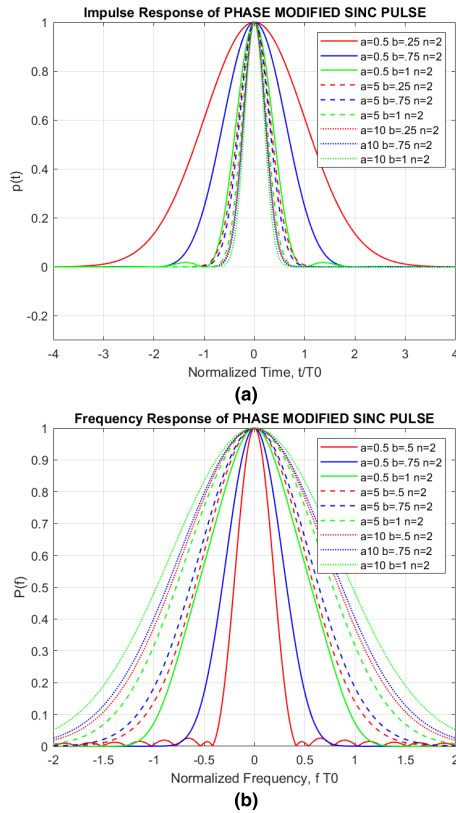and the PLCP impulse and frequency response are shown in Fig. 11.

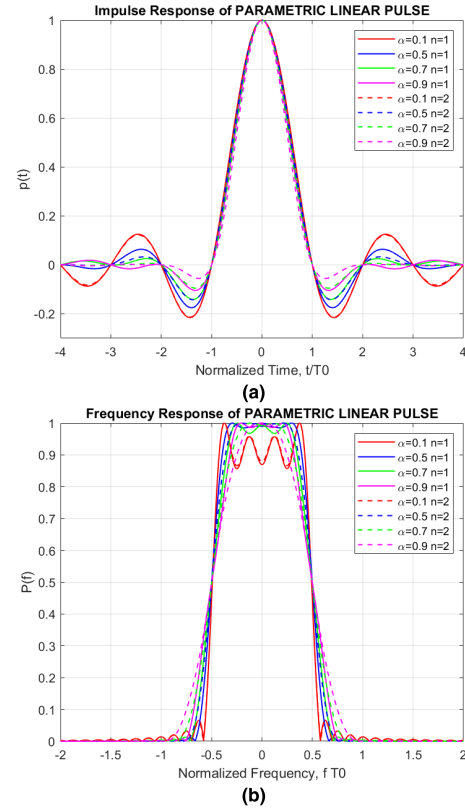**FIGURE 8.** (a) Impulse and (b) frequency response of PMSP for n = 2.



**FIGURE 9.** (a) Impulse and (b) frequency response of PLP for n = 1, 2.

### 9) PHYDYAS FILTER

This PF was first developed in [90] and investigated in [37]. Then it was employed as the PF in the European PHYDYAS project on FBMC [38].

This filter contains 2K-1 filter frequency taps, K represents the overlapping factor with the adjacent subchannel [91]. The continuous frequency response of the PHYDYAS filter is given as follows

$$P(f) = \sum_{k=-(K-1)}^{K-1} H_k \frac{\sin(\pi(f - \frac{k}{MK})MK)}{MK \sin(\pi(f - \frac{k}{MK}))} \quad (46)$$

where $f$ is the continuous frequency domain. $H_k$ coefficients are the values of $P(f)$ at certain frequencies which are optimized and extracted in the design process [38]. The impulse response obtained as

$$p_{PHYDYAS} = 1 + 2 \sum_{k=0}^{K-1} H_k \cos(2\pi \frac{kt}{KT_0}) \quad (47)$$

Fig. 12 shows the impulse and frequency response of PHY-DYAS for overlapping factors K= 4, 6 and 8.

### 10) HERMITE FILTER

The Hermite pulse shaping filter is given form the linearly combining of the function of the Hermite Gaussian which achieves the Nyquist-I criterion [92]. Thereby, the Hermite

PF coefficients are given by Hermite polynomials in [92]. The Hermite filter impulse response can be described by

$$p_{hermite} = \frac{1}{\sqrt{T_0}} \exp\left(-2\pi \left(\frac{t}{T_0}\right)^2\right)$$
$$\times \sum_{\substack{i = \{0, 4, 8, \\ 12, 16, 20\}}} a_i H_i \left(2\sqrt{\pi} \frac{t}{T_0}\right) \quad (48)$$

The Hermite filter impulse and frequency response are shown in Fig. 13.

### B. BLOCK SPREAD FBMC/OQAM

Compared to OFDM, FBMC provides superior spectral properties at the cost of imaginary interference, making MIMO implementation more difficult. By time or frequency spread of the symbols, the imaginary interference can be completely removed, so, all OFDM MIMO methods can be implemented directly in FBMC [67].

Our model is based on the idea of literature [75], [76] which uses Hadamard matrices in the spreading process for enabling low complexity. As in [75], the Balian-Low theorem has been satisfied by applying the orthogonality for real symbols only $x_{m,n} \in \mathbb{R}$, instead of the complex orthogonality, which leads to relax the orthogonality situation [93]. If both time and frequency spacing reduced by 2, $T_0F=1/2$ for real-valued
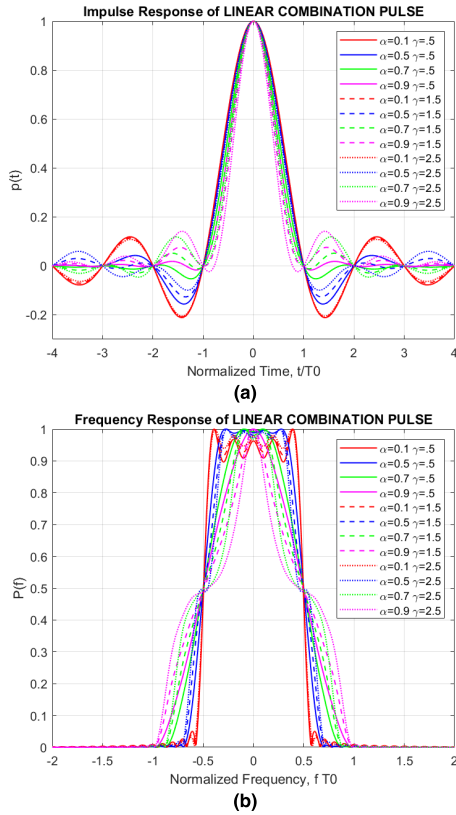
**FIGURE 10.** (a) Impulse and (b) frequency response of LCP for $\gamma = 0.5$, $1.5$ and $2.5$ and $\alpha = 0.1$, $0.5$, $0.7$ and $0.9$.



**FIGURE 11.** (a) Impulse and (b) frequency response of PLCP for $\mu = 1.2$, $1.6$ and $2.5$ and $\alpha = 0.1$, $0.5$, $0.7$ and $0.9$.

symbols, then complex symbols $T_0F=1$. This frequency-time squeezing causes interference, but this is shifted by the phase shift $\theta_{m,n} = \frac{\pi}{2}(m+n)$ to the purely imaginary domain. Then, by taking only the real part, the imaginary interference is completely removed.

Fig. 14 illustrates the conventional FBMC transmission idea. Real-symbols can be transferred over a time-frequency rectangular position. The primary issue with FBMC is imaginary interference. This issue can be avoided by spreading data symbols over multiple time gird or several subcarriers, see Fig. 15 and 16, which enables the transmission of complex symbols with blocking of the imaginary interference.

For the AWGN channel, the received PF matrix can be written as $\boldsymbol{Q^H} = \boldsymbol{G^H}$, and, $\boldsymbol{H} = \boldsymbol{I_N}$, then, (20) transforms to

$$\boldsymbol{y} = \boldsymbol{G^H G r} = \boldsymbol{Dx} + \boldsymbol{n} \qquad (49)$$

where $\boldsymbol{D} = \boldsymbol{G^H G}$ is the transmission matrix and $n \sim \mathcal{CN}(0, P_n D)$ is random noise.

Note that (49) shows a block of M subcarriers and N symbols transmission.

In order to attain a required bandwidth and transmission time, some of these blocks should be concatenated in frequency and time. For block spreading, the spreading/coding matrix $C \in \mathbb{C}^{MN \times \frac{MN}{2}}$, is used to precode the complex symbols $\tilde{x} \in \mathbb{C}^{\frac{MN}{2} \times 1}$, so the transmitted data symbols $x \in \mathbb{C}^{MN \times 1}$
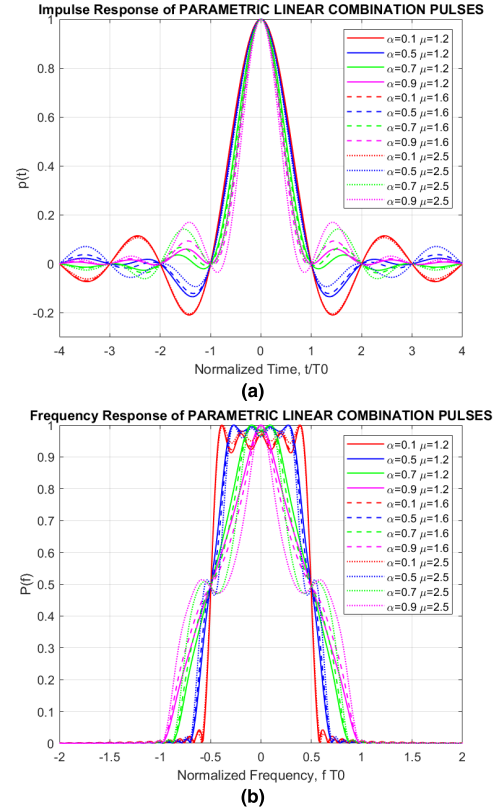
are obtained by

$$\boldsymbol{x} = \boldsymbol{C\tilde{x}} \qquad (50)$$

and the received data symbols $\tilde{y}$ are produced by decoding the received symbols

$$\boldsymbol{\tilde{y}} = \boldsymbol{C^H y} \qquad (51)$$

To maintain the complex orthogonality, the spreading matrix $C$ must satisfy the following situation.

$$\boldsymbol{C^H D C} = \boldsymbol{I} \qquad (52)$$

Off-diagonal elements will represent imaginary interference, the identity matrix will be $\Re\{D\} = I_{MN}$ only by taking the real part [75]. By taking an eigendecomposition of the transmission matrix $D = G^H G = U \Lambda U^H$ with the unitary matrix U, we avoid losing any information that may cause by taking only the real part. For $M \to \infty$ and $N \to \infty$, D has just $MN/2$ eigen-values with value equal 2. Therefore, only $MN/2$ complex data symbols are transmitted, that is equal to transmit $MN$ real data symbols.

This condition (52) can be satisfied by applying an eigenvalue decomposition, but this approach will be a high number of computational and complexity. To enable low complexity, we use $M \times M$ Hadamard matrix and data symbols spreading over $M/2$ column vectors of a matrix in time. A spreading matrix $C \in \mathbb{R}^{MN \times \frac{MN}{2}}$, that satisfies the condition in (52),

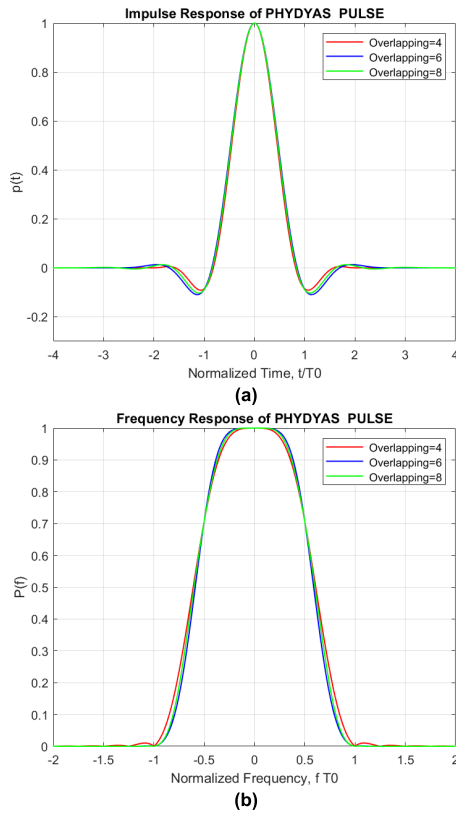**FIGURE 12.** (a) Impulse response and (b) frequency response of PHYDYAS for overlapping factors K = 4, 6 and 8.
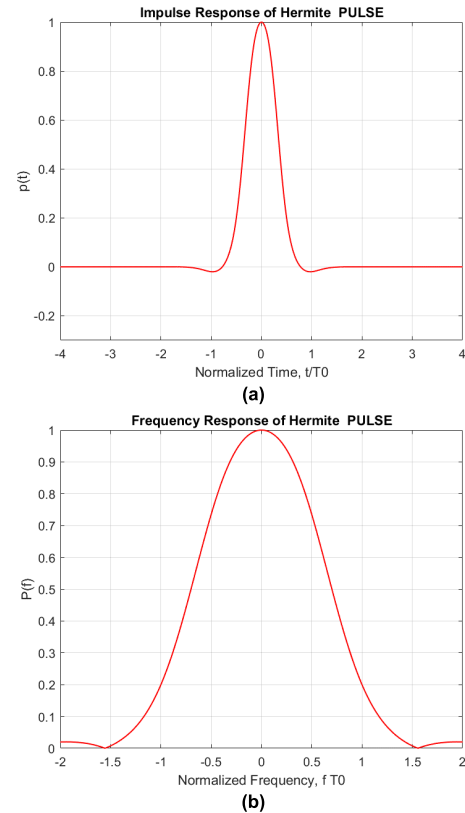


**FIGURE 13.** (a) Impulse response and (b) frequency response of Hermite for overlapping factors K = 4, 6 and 8.

can be found in [76]. While the big advantage of Hadamard spreading is no multiplications required but only additions, so that the complexity is increased slightly, a drawback is the length of the coding must be a power of two. This makes it hard to integrate within systems, but when a system is built from scratch, it has almost no effect [67].

### 1) WALSH–HADAMARD SPREADING IN FREQUENCY

The flat frequency channel for a length of spreading and flat time within one symbol is assumed to enable low complexity equalizer. We apply a guard subcarrier to separate between frequency blocks as in [75]. We can rewrite the coding matrix C to satisfy the condition as (52) (as a spread over frequency only) [75]:

$$C = I_N \otimes C_0 \tag{53}$$

The frequency spreading matrix for a one-time slot is described by $C_0 \in \mathbb{R}^{N \times \frac{N}{2}}$. By taking every second column out of a sequency order WH matrix $\mathcal{H} \in \mathbb{R}^{N \times N}$ [94], we can get the coding matrix $C_0$:

$$[C_0]_{n,r} = [\mathcal{H}]_{n,2r} \; \textit{for } n = 1 \ldots N; r = 1 \ldots \frac{N}{2}. \tag{54}$$

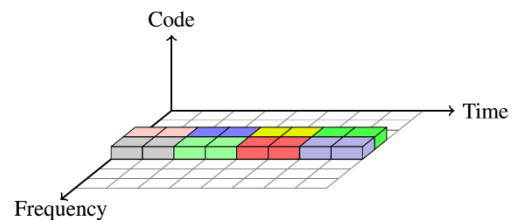In [75], an example of the coding matrix is provided.



**FIGURE 14.** Conventional FBMC/OQAM transmission where only real symbols can be positioned [76].
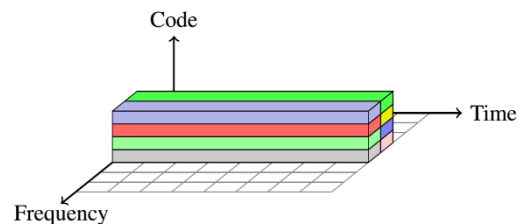


**FIGURE 15.** Coded FBMC/OQAM transmission where complex symbols are spread over multiple time slots [76].

### 2) WALSH–HADAMARD SPREADING IN TIME

The coding matrix for spreading in time can be provided by $C_1 \in \mathbb{R}^{N \times \frac{N}{2}}$ and $C_2 \in \mathbb{R}^{N \times \frac{N}{2}}$ where one has to switch between $C_1$ and $C_2$ for neighboring subcarrier. Each second column from WH sequency $\mathcal{H} \in \mathbb{R}^{N \times N}$ is taken to get
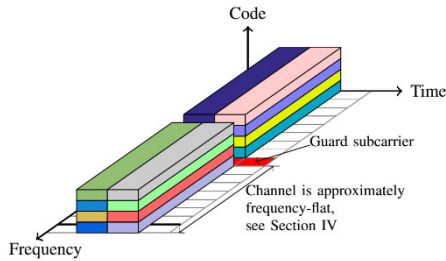
**FIGURE 16. Coded FBMC/OQAM transmission where complex symbols are spread over multiple frequency subcarriers. Different frequency blocks are separated by a guard subcarrier [75].**

**TABLE 1. The optimum parameters for each filter.**

| Pulse Shaping Filter | Parameters |
|---|---|
| RC | $\alpha=0.9$ |
| RRC | $\alpha=0.9$ |
| BTRC | $\alpha=0.9$ |
| MBH | $\alpha=0.9, \beta=1.2$ |
| ISP | $a=5, n=1$ |
| PMSP | $a=5, b=1, n=1$ |
| PLP | $\alpha=0.9, n=2$ |
| LCP | $\alpha=0.9, \gamma=1.5$ |
| PLCP | $\alpha=0.9, \mu=1.6$ |
| PHYDYAS | $K=4$ |
| Hermite | - |

coding matrix in time [76], [94].

$$[C_1]_{n,r} = [\mathcal{H}]_{n,2r-1} \text{ and } [C_2]_{n,r} = [\mathcal{H}]_{n,2r}$$
$$\text{for n=1...N;r=1...}\frac{N}{2} \quad (55)$$

We can get the coding matrix $C \in \mathbb{R}^{MN \times \frac{MN}{2}}$ by vectorization.

$$C = C_1 \otimes I_{M/2} \otimes \begin{bmatrix} 1 & 0 \\ 0 & 0 \end{bmatrix} + C_2 \otimes I_{M/2} \otimes \begin{bmatrix} 0 & 0 \\ 0 & 1 \end{bmatrix} \quad (56)$$

The orthogonality condition in (52) can be satisfied by (56).

## IV. RESULTS AND DISCUSSIONS

In this section, the performance of the proposed prototype pulse shaping filters in FBMC/OQAM systems is evaluated via simulation results obtained using MATLAB 2018a software. Furthermore, the validity of our proposed filters with proposed approaches in MIMO systems is verified.

### A. PROTOTYPE PULSE SHAPING FILTER ANALYSIS

In this subsection, we compare all pulse shaping filters analysed in section III in terms of their impulse response and frequency response. The results can allow the selection of a well-localized pulse in the time and frequency domains. Through extensive computer simulations, the optimum constants and parameters for each filter can be found, as shown in Table 1.
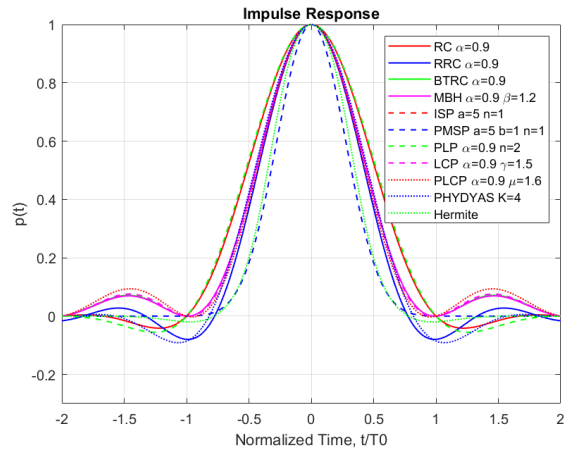


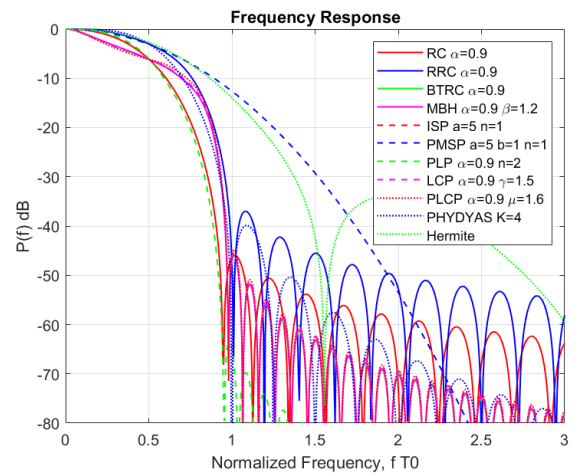**FIGURE 17. Comparison of the impulse response of the proposed PFs.**



**FIGURE 18. Comparison of the frequency response of the proposed PFs.**

Figs. 17 and 18 show a comparison of the impulse and frequency responses of all proposed pulse shaping filters. As illustrated in Fig. 17, all pulse shaping filters have almost equal main lobe width; however, the Hermite and PMSP pulse shaping filters have narrower and lower sidelobe levels, whereas the remaining pulse shaping filters have almost equal sidelobe levels. The impulse response of Hermite and PMSP decays rapidly. The prior observation is very important because a pulse with smaller sidelobes is desired to minimize errors due to ISI, obtain a larger eye opening, minimize the maximum distortion due to ISI, and minimize the PAPR of the system.

Fig. 18 shows the frequency responses of the pulse shaping filters. All pulses retain the same bandwidth, excluding the Hermite and PMSP. The sidelobe is maximum for the Hermite pulse and minimum for PLP, as the sidelobe contains the ICI power. This property of the PLP will reduce ICI compared with the other filters. Overall, a trade-off exists between an impulse response with smaller sidelobes and its spectral magnitude.

## B. POWER SPECTRAL DENSITY ANALYSIS

The good localization of the spectrum of the transmitted signal is the primary benefit of the FBMC technique, which causes a reduction in the OoB emissions and improves spectral characteristics. The PSD is defined as the content of power in the signal versus the frequency range. The FBMC signal has a coefficient of the PFs as one of its components. Therefore, OoB emissions can be reduced by selecting the appropriate PF.

The expected transmit power in time can be calculated using matrix representation, $P_S \in \mathbb{R}^{N \times 1}$ [60]:

$$P_S = diag\{GR_x G^H\} \quad (57)$$

where $R_x = \mathbb{E}\{xx^H\}$ describes the correlation matrix of the transmitted symbols.

The PSD, $PSD \in \mathbb{R}^{N \times 1}$ can also be calculated by

$$[\boldsymbol{PSD}]_j = \sum_{i=0}^{MN-1} \left| \left[ \boldsymbol{WGU}\sqrt{\Lambda} \right]_{j,i} \right|^2 \quad (58)$$

where W is a DFT matrix while U and $\Lambda$ are obtained an Eigen decomposition of $R_x = U\Lambda U^H$ and $U\sqrt{\Lambda} = I_{MN}$, that is, in many cases $R_x$ is an identity matrix. It can also calculate the average transmit power to get normalize PSD,

$$\bar{P}_S = \frac{1}{MT_0} tr\{GR_x G^H\}\frac{1}{f_s} \quad (59)$$

$tr\{.\}$ is a trace operator, and $f_s = FN_{FFT}$ is the sampling rate, where $N_{FFT} \geq M$ represents FFT size.

For FBMC/OQAM and CP OFDM, the SNR can be expressed by [60]:

$$SNR = \frac{\bar{P}_S}{MFN_0} \quad (60)$$

where $N_0 = P_n/f_s$ is the noise power spectral density.

Simulations are performed to check the PSDs and make comparisons of the PSD efficiency of the proposed PFs. Let just one subcarrier m is assumed to be active. In this simulation, we set the parameters as follows: i) subcarrier spacing F (15 kHz, same as LTE); ii) number of subcarriers M=24; iii) number of FBMC symbols N=105; iv) modulation order of 16 QAM; v) filters parameters as shown in Table 1; and vi) OFDM as in [60]. We only consider the transmitted date on the first subcarrier because the PSD is calculated from the summation of all subcarrier that represents the frequency-shifted version of the first one. The simulated PSDs are acquired by inserting arbitrary symbols to FBMC/OQAM and then evaluating the transmitted signal PSDs for each PF.

Fig. 19 shows the transmitted power of FBMC/OQAM considering the PFs, which is calculated according to (59). Fig. 20 illustrates the PSDs of the OFDM and FBMC/OQAM systems with the proposed PFs. The estimation is based on computing the FFT of 200 blocks of the transmitted signal.

Clearly, FBMC/OQAM achieve good spectral characteristics relative to CP-OFDM, in which the rectangular pulse that is used in OFDM, causing high OoB radiations, and we
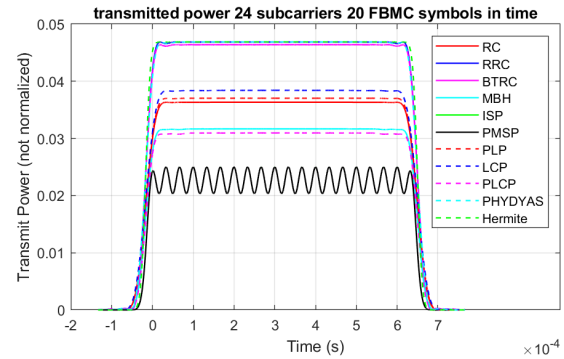
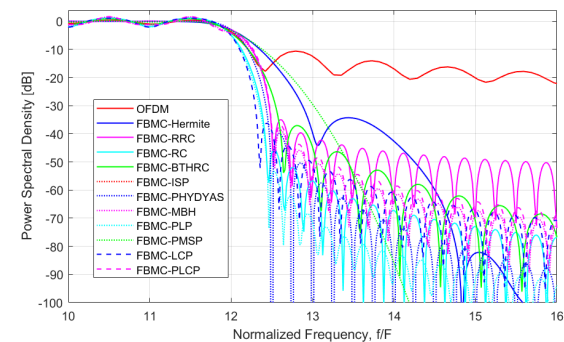**FIGURE 19.** Comparison of the transmitted power of the FBMC/OQAM using proposed PFs.

**FIGURE 20.** Comparison of PSD of the FBMC/OQAM using proposed PFs.

observe that the power of FBMC-OQAM in the OoB region is lower than that of CP-OFDM. Additionally, PLP and LCP achieve the best spectral properties and lower OoB emissions than all the other PFs, and this result verifies the best spectral properties of PLP and LCP shown in Fig. 18. PHYDYAS has the sharpest edges but has more sidelobes than PLP and LCP.

The Hermite and RRC pulses have greater OoB emissions compared to the other pulse shaping filters, but these emissions are still better than those of OFDM.

## C. POSSIBLE USE SCENERIES FOR FBMC

In this subsection, we discuss how FBMC can be utilized to efficiently support different use cases, envisioned for future wireless systems. We start with a definition of the time frequency efficiency. Then, we assume that two users with two different subcarrier spacing share the same band and calculate the SIR. The time frequency efficiency helps to answer the question of which modulation format utilizes available time-frequency resources best.

### 1) SPECTRAL EFFICIENCY

Here, the PFs will be investigated in FBMC and their performances discussed in terms of the time-frequency efficiency, which is defined as:

$$\rho = \frac{NM}{(NT_0 + T_G)(FM + F_G)} \quad (61)$$

where $T_G$ is the guard interval and $F_G$ is the guard band.

Fig. 21 shows the time-frequency efficiency over the number of subcarriers M for the proposed PFs with $N = 2$, $N = 10$
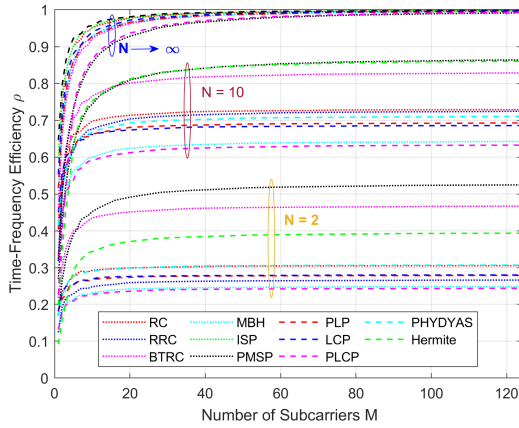
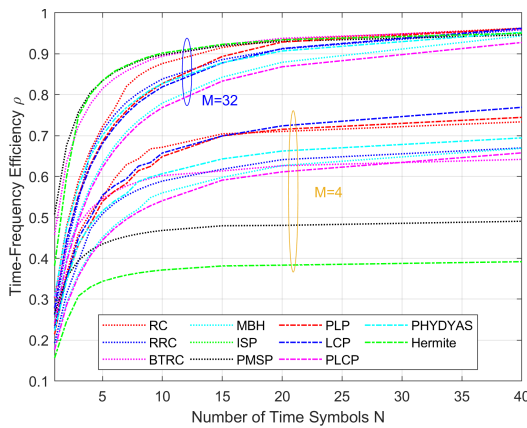**FIGURE 21.** Time-frequency efficiency for N=2, N=10, and N→ ∞.



**FIGURE 22.** Time-frequency efficiency for M=4 and M=32.

and $N \rightarrow \infty$. The time interval $NT_0 + T_G$ depends on the guard time $T_G$, which is chosen so that 99% of the energy is transmitted. As FBMC requires a large guard time due to the filter length, choosing a PF that improves this issue is significant.

As illustrated in Fig. 21, the comparison reveals that for N=2, PMSP and ISP show better performance than all the other types, and as N increases, the time-frequency efficiency increases because of the decreasing guard time relative to the PF length, while this phenomenon relies on the subcarrier number.

Additionally, in the case of a large number of symbols $N \rightarrow \infty$, all types of PFs achieve nearly the same performance. Fig. 22 shows the time-frequency efficiency over the number of time symbols N for the proposed PFs with M=4 and M=32. PLP and LCP can achieve better efficiency for M=4. Similar to Fig. 21, increasing M leads to increasing time-frequency efficiency due to decreasing guard frequency.

### 2) SIGNAL-TO-INTERFERENCE RATIO (SIR)

The SIR may be used to evaluate the point where interference starts to overtake noise. In this section, two adjacent users and no channel are assumed for simplicity. The first user has $M_1 = 96$ subcarriers with a subcarrier spacing $F_1 = 15$ kHz, the second user has $M_2 = 12$ subcarriers and a subcarrier
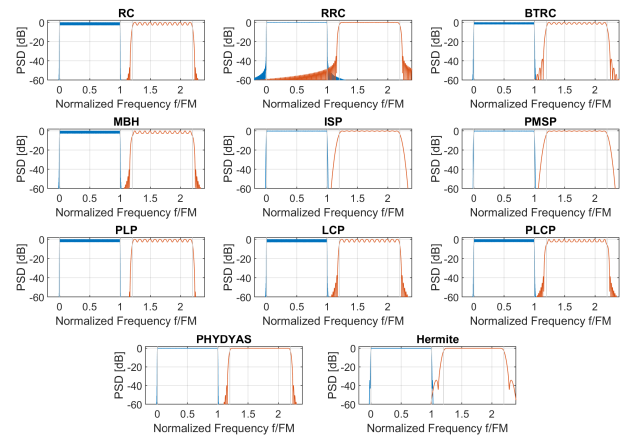


**FIGURE 23.** PSD for two users with a subcarrier spacing (F $_1$ = 15 KHz and F $_2$ = 120 KHz) share the same band.
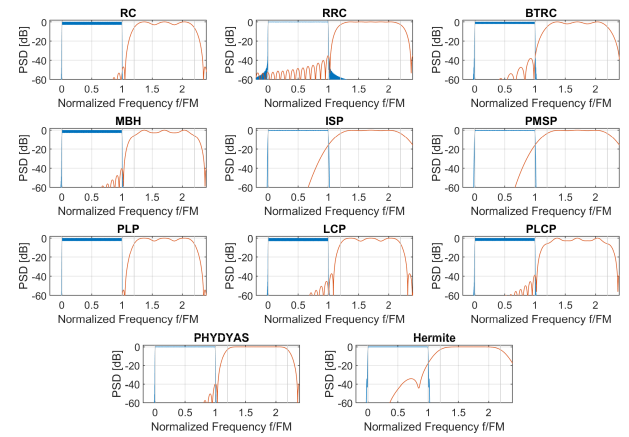


**FIGURE 24.** PSD for two users with a subcarrier spacing (F $_1$ = 15 KHz and F $_2$ = 480 KHz) share the same band.

spacing $F_2 = 120$ kHz or $F_2 = 480$ kHz, and for both users, $F_G = 0.25 F_1 M_1$. As a result, the bandwidth for both users is 1.44 MHz. Figs. 23 and 24 show the PSD for the two users with the proposed subcarrier spacings $F_1 = 15$ kHz and $F_2 = 120$ kHz and $F_1 = 15$ kHz and $F_2 = 480$ kHz, respectively. Our results show that interference increases with increasing subcarrier spacing, as seen by comparing Fig. 23 with Fig. 24. The results demonstrate two things. First, the interference insertion from the first user to the second user is lower than the second user interference inserting to the first user because of the filter length of user 2 ($M_2 = 12$) is shorter than that of the first user ($M_1 = 96$). Second, a larger subcarrier spacing ($F_2 = 480$ kHz) causes larger interference. From the results in Fig. 24, the OoB emissions for PLP and LCP are lower than those for the other filters, which leads to small interference between users. This result confirms the findings obtained with the PSD results in Fig. 20. SIR is calculated as [60]:

$$SIR_{two\ user} = \frac{M_1 N_1 + M_2 N_2}{\left\| \Re \left\{ Q_1^H G_2 \right\} \right\|_F^2 + \left\| \Re \left\{ Q_2^H G_1 \right\} \right\|_F^2} \quad (62)$$

where $\| . \|_F$ is the Frobenius norm [44].

**FIGURE 25.** Comparison of SIR evaluation for different types of filters in the case of two users with a subcarrier spacing ($F_1 = 15$ KHz and $F_2 = 120$ kHz).



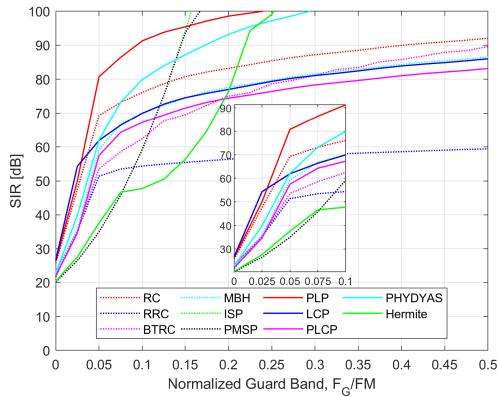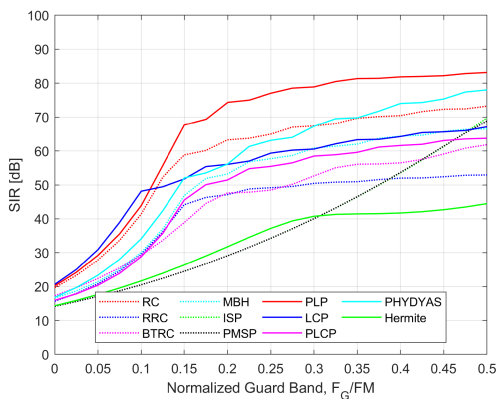**FIGURE 26.** Comparison of SIR evaluation for different types of filters in the case of two users with a subcarrier spacing ($F_1 = 15$ KHz and $F_2 = 480$ kHz).

Figs. 25 and 26 show the effect of the guard band on the SIR, where the guard time is ignored, as a lower inference is observed with a higher guard band.

In the case of $F_2 = 120$ kHz (Fig. 25), assuming that SIR=60 dB is required, for PLP, the guard band $F_G = 0.03$FM is required to achieve the target SIR, with $\rho = 1/1.03 = 97\%$, and for LCP, $F_G = 0.045$FM, with $\rho = 95.7\%$. In the same manner, we can obtain $\rho = 91\%$ for PMSP and $\rho = 85.47\%$ for Hermite. For the RRC filter, The SIR is below 60 dB. In the case of $F_2 = 480$ kHz (see Fig. 26), increasing the subcarrier spacing causes additional interference. In the same manner, PLP can improve the SIR by approximately 40 dB over Hermite at $F_G = 0.25$FM, this decreases the needed guard bands compared to other filters.

The results lead to a similar conclusion that the proposed PLP introduces less SIR than Hermite. As shown in Fig. 26, increasing the subcarrier spacing requires a higher guard band. The higher subcarrier spacing, which is assigned for the second user, is to allow low latency transmissions. Thus, in particular, the comment that low latency in FBMC cannot be adequate is not accurate. The subcarrier spacing only should be increased to improve this issue. Indeed, the effects
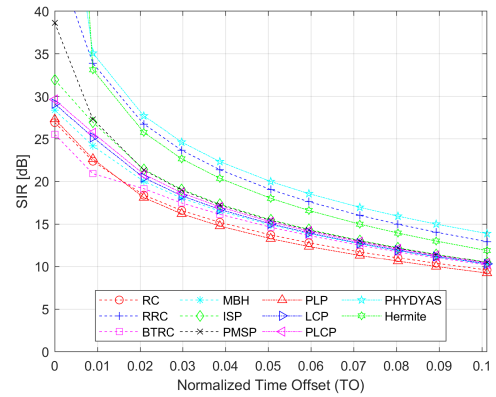


**FIGURE 27.** SIR in presence of time-offset for proposed PFs.

of the TOs and the channel delay spread will be increased but the sensitivity to CFOs and channel Doppler spreads will be reduced.

### D. TIME OFFSETs (TOs) AND CARRIER FREQUENCY OFFSETs (CFOs)

Multicarrier techniques are sensitive to synchronization offset. A TO and a CFO can destroy the orthogonality between subcarriers and cause ISI. A TO is caused by the non-perfect alignment of baseband samples in time, which occurs due to channel propagation delay. Of course, the system needs time synchronization methods. However, the mMTC system should avoid time advanced mechanisms, such as LTE [28], to decrease power consumption and enhance spectral properties.

Here, we will evaluate the SIR in the presence of a TO/CFO in FBMC/OQAM using the proposed filters, with the following parameters: i) M=48; ii) N=8; iii) F=15 kHz; and iv) BW=M*F=0.72 MHz. Fig. 27 shows SIR values for normalized TOs $t^*_{offset}$F. A gain of 7 dB is noticed with PHYDYAS relative to PLP or RC for a normalized TO of 0.05, and an approximately 4 dB difference between Hermite, PHYDYAS or RRC and the other PFs is found. Clearly, PHYDYAS attains a greater SIR than the other PFs because in the frequency domain the PHYDYAS PF has very sharp edges. The sensitivity of communication systems to a CFO is an important issue because it can result in ICI. The SIR in the presence of a CFO is shown in Fig. 28, which shows that Hermite is slightly better than the other filters that have symmetrical frequency and time shape.

### E. BIT-ERROR-RATE PERFORMANCE OVER VARIOUS CHANNELS

In this subsection, the BER performance of the FBMC waveform with the proposed PFs compared to OFDM is provided through simulations. The simulation parameters are summarized in Table 2. We assume perfect synchronization and no TO or CFO; three channels are used for the simulation: (a) AWGN; (b) extended Pedestrian A channel model (EPA); and (c) extended Vehicular A channel model (EVA) [95]. We use these channels models because the EPA and EVA
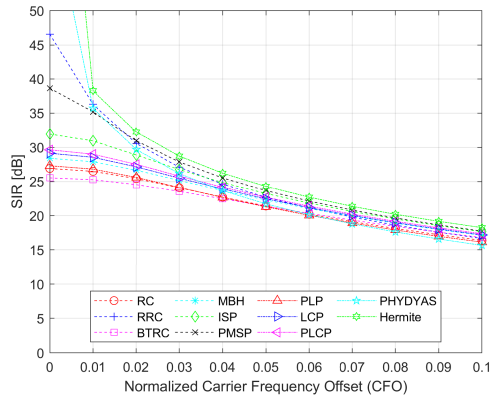
**FIGURE 28.** SIR in presence of carrier frequency offset (CFO) for different PFs.

**TABLE 2.** Simulation parameters.

| Simulation Parameters | Value |
|---|---|
| Modulation Order | 16 and 256 QAM |
| Number of Symbols (N) | 30 |
| Number of Subcarriers (M) | 24 |
| Subcarrier Spacing (F) | 15 KHz |
| Overlapping factor (K) | 4 |
| Carrier Frequency (fc) | 2.5 GHz |
| Channels model | AWGN, EPA, and EVA |
| Doppler frequency shift ($f_D$) | 5Hz for EPA |
|  | 300Hz for EVA |

channel models describe the practice of present and future channel model in mobile systems [96].

The BER is calculated for OFDM as in [97], [98] and for FBMC according to [67] based on one tap ZF equalization, which eliminates self-interference but introduces noise that depends on the choice of PF. The theoretical BER for OFDM has been plotted as a benchmark to prove the validity of the BER curves[97], [98].

Since the FBMC uses PF to filter each subcarrier, the tail of the filter is much longer than OFDM which causes FBMC not suitable for small packet transmission and low latency sceneries. In FBMC, the duration of the symbol is greater than the maximum delay spread, even, the ISI can be caused by interference between the low magnitude of the signal and the next symbol which will yield very small ISI. Thus, there is no ISI-mitigation scheme is adopted for FBMC. The efficiency reduction due to ISI is therefore low and can be neglected [99].

Figs. 29-31 depict the BER performance over the SNR for two different modulation orders (16 and 256 QAM) through the AWGN, EPA, and EVA channels. As expected, a lower modulation order achieves better performance than a higher order. However, performance degradation can be observed for high-order modulation because the dense constellation makes it more sensitive to the ISI. Despite the ISI, performance degradation is very tiny because the ISI power is very small.

FBMC for all PFs and OFDM for AWGN have nearly the same BER for 16 QAM, as shown in Fig. 29. Similar
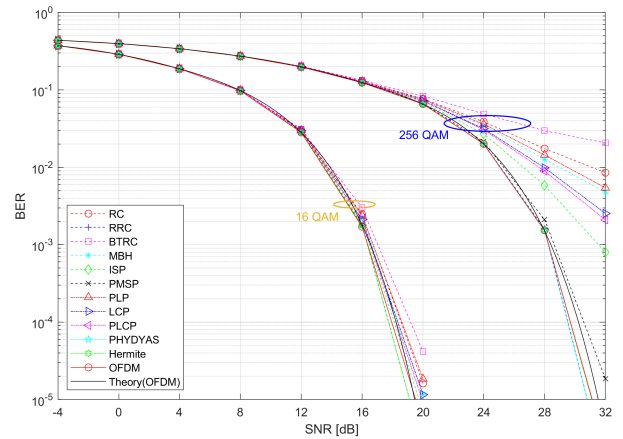


**FIGURE 29.** BER performance of FBMC with proposed PFs relative to CP-OFDM over the AWGN channel for modulation order 16 and 256 QAM.



**FIGURE 30.** BER performance of FBMC with proposed PFs relative to OFDM over EPA channel with $f_D = 5$Hz for modulation order 16 and 256 QAM.



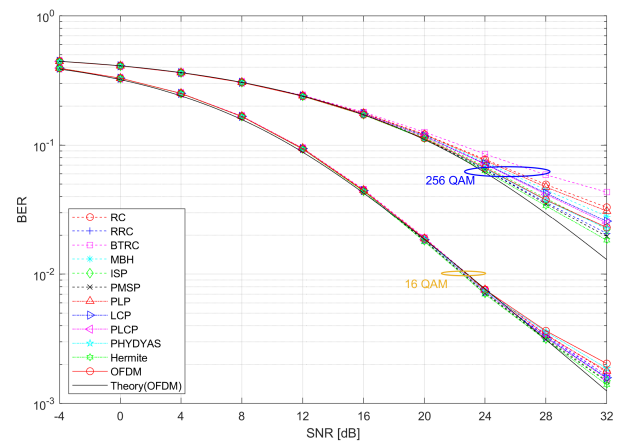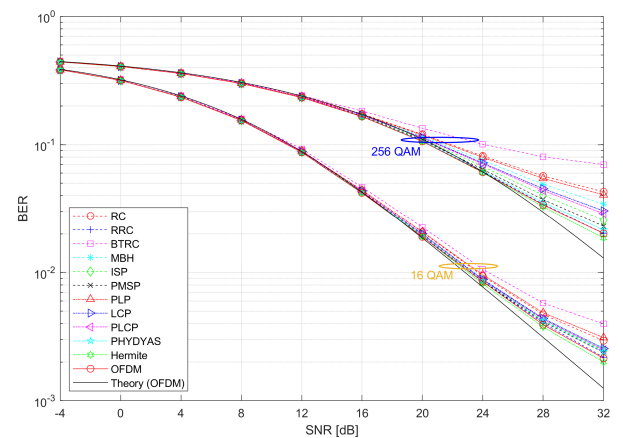**FIGURE 31.** BER performance of FBMC with proposed PFs relative to OFDM over EVA channel with $f_D = 300$Hz for modulation order 16 and 256 QAM.

conclusions can be seen for the EPA and EVA channels, as shown in Figs. 30 and 31. However, for 256 QAM, OFDM and FBMC using PMSP, PHYDYAS, Hermite and RRC outperform the other PFs for a high SNR in the AWGN channel, as shown in Fig. 29.
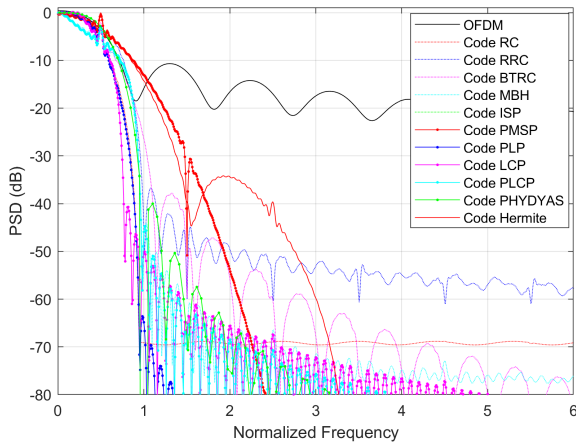
**FIGURE 32.** PSD of Coded FBMC vs. Normalized frequency f/F (applying the WH frequency spreading), the unique spectral properties of FBMC are still maintained.

As the EPA channel model has a moderate delay spread, we provide the performance results in Fig. 30. We note that we get much the same results as CP-OFDM for all PFs in FBMC. In the case of the EVA channel (Fig. 31), the Doppler spread drives the interference, so FBMC (all filters except BTRC) performs better than OFDM. Due to the relatively high delay spread in the EVA channel, FBMC deviates at high SNR values. However, for SNR ranges below 20 dB, this issue does not arise. The simulations validate that the proposed PFs in the FBMC/OQAM transmission system has nearly the same BER compared with the traditional PFs and as OFDM for 16 QAM and perform better than OFDM for 256 QAM in the high SNR region. Moreover, FBMC has the added advantage of greater spectral properties due to the reduction in OoB emissions.

### F. MIMO SIMULATIONS

We exploit the WH spreading in time or frequency, as explained earlier, to restore the complex orthogonality of the FBMC/OQAM system, as the Alamouti coding scheme requires the complex orthogonality property. Our MIMO FBMC/OQAM scheme applies not only to the Alamouti scheme but also to well-known MIMO methods that can be combined with our model such as the SM scheme.

In this subsection, we verify the validity of our proposed prototype pulse shaping filters in terms of the BER with the MIMO system for the Alamouti scheme, SM with ZF detection and SM with ML detection using the WH spreading method in different channel models. Furthermore, we compare our results with other prototype pulse shaping filters and with CP-OFDM as a benchmark to prove the validity of our models in MIMO.

A fast WH transform transformation can decrease computational complexity [100]. Hence, $\log_2(N) - 1$ extra additions or subtractions are needed at the transmitter for each complex symbol, and $\log_2(N)$ extra additions or subtractions are also needed at the receiver. The WH approach's only minor drawback is that the length of spreading should be a power of two. Furthermore, apart from a few tiny ripples, WH spreading
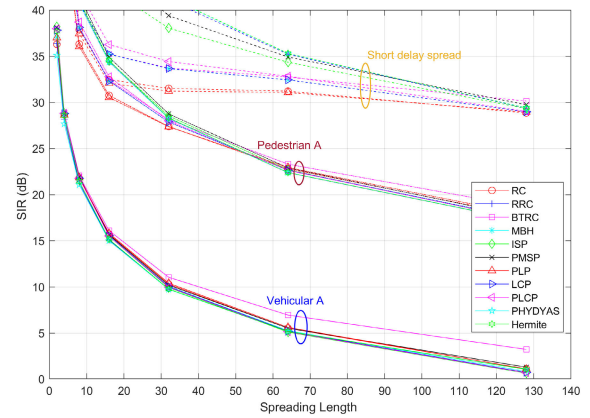


**FIGURE 33.** SIR performance for FBMC proposed PFs using with different spreading length under three different channel delay spread (10 ns, 46 ns Pedestrian A channel and 370 ns Vehicular A).

**TABLE 3.** Simulation parameters.

| Parameter | Value |
|---|---|
| Modulation Order | 16 |
| Number of Symbols (N) | 32 |
| Number of Subcarriers (M) | 2 to 128 |
| Subcarrier Spacing (F) | 15 KHz |
| Carrier Frequency (fc) | 2.5 GHz |
| Number of guard subcarriers | 1 (spreading in frequency) |
| Number of guard symbols | 3 (spreading in time) |
| Channel models [101] | Short delay spread of 10 ns. |
| | Pedestrian A (delay spread of 46 ns). |
| | Vehicular A (delay spread of 370 ns). |
| Doppler spread | Jakes Doppler spectral density |

has almost no impact on the PSD (see Fig. 32), so FBMC's superior spectral properties are maintained. As we can notice that PSD in fig. 32 is the same as the PSD in Fig. 20 with a few ripples.

#### 1) WALSH-HADAMARD SPREADING IN FREQUENCY

First, the impact of a Rayleigh fading channel is investigated, we neglect the noise in frequency spreading scheme, so that (49) transforms to:

$$\tilde{y} = C^H G^H HGCx \tag{63}$$

where $H \in \mathbb{C}^{N \times N}$ is a time-variant channel matrix.

In [75], an analytical SIR expression is derived in a doubly-flat Rayleigh channel:

$$SIR_{m,n} = \frac{[\Gamma]_{i,i}}{tr\{\Gamma\} - [\Gamma]_{i,i}} \tag{64}$$

where

$$i = \frac{M}{2}(n-1) + r, \tag{65}$$

$$\Gamma = \left((GC)^T \otimes \left(c_{r,n}^H G^H\right)\right) R_{vec\{H\}} \left((GC)^T \otimes \left(c_{r,n}^H G^H\right)\right)^H \tag{66}$$
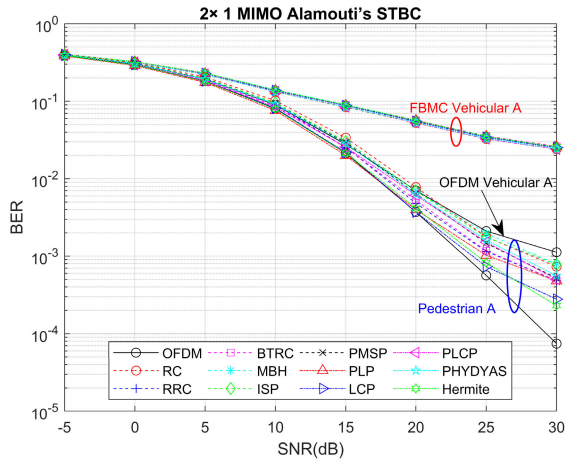
**FIGURE 34.** BER performance comparison between CP-OFDM and WH block frequency spreading FBMC using different PFs in 2 × 1 Alamouti's STBC scheme over the Pedestrian A and Vehicular A channel model.



**FIGURE 35.** BER performance comparison between CP-OFDM and WH block frequency spreading FBMC using proposed PFs in 2 × 2 MIMO scheme using ZF detection over the Pedestrian A and Vehicular A channel model.



**FIGURE 36.** BER performance comparison between CP-OFDM and WH block frequency spreading FBMC using proposed PFs in 2 × 2 MIMO scheme using ML detection over the Pedestrian A and Vehicular A channel model.



**FIGURE 37.** BER performance comparison between CP-OFDM and WH time spreading FBMC using proposed PFs in 2 × 1 Alamouti's STBC scheme over the Pedestrian A and Vehicular A channel model.



**FIGURE 38.** BER performance comparison between CP-OFDM and WH time spreading FBMC using proposed PFs in 2 × 2 MIMO scheme using ZF detection over the Pedestrian A and Vehicular A channel model.
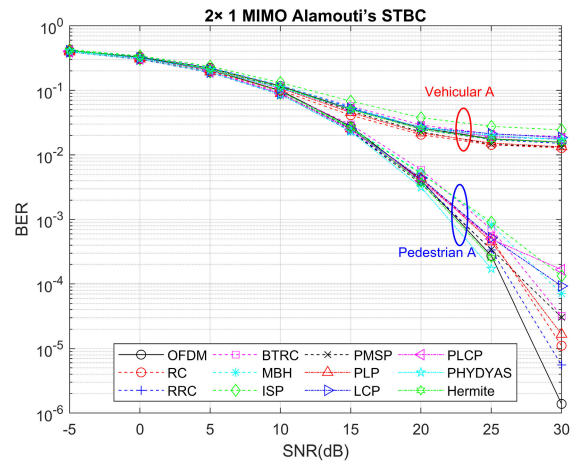


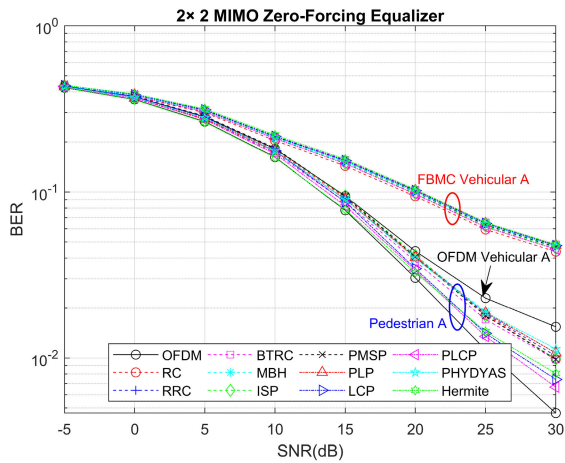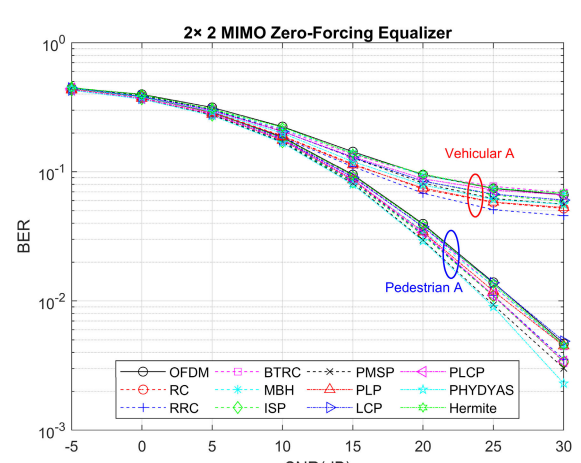**FIGURE 39.** BER performance comparison between CP-OFDM and WH time spreading FBMC using proposed PFs in 2 × 2 MIMO scheme using ML detection over the Pedestrian A and Vehicular A channel model.
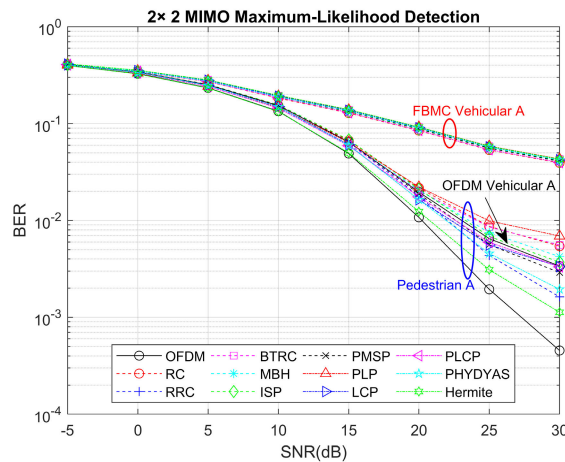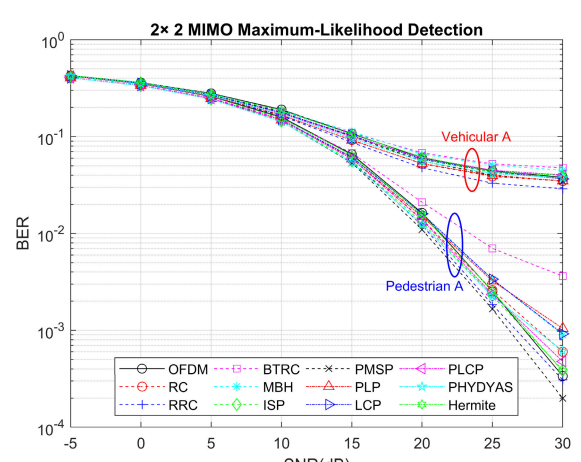
where $c_{r,m} \in \mathbb{R}^{N \times 1}$ is the i$^{th}$ column of $C$ for $i = M/2(n-1)+r$ and $R_{vec\{H\}} = \mathbb{E}\left\{vec\{H\} vec\{H\}^{H}\right\}$ is the correlation matrix that contains the statistical properties of the channel delay profile and Doppler spread.

Simulation results for the SIR values with different spreading lengths for each considered PF can be found in Fig. 33. While the parameters of the simulation are summarized in Table 3.

Fig. 33 shows how the SIR depends on the spreading length. We can observe that the interference increases with increasing the length of spreading. However, the spectral efficiency increases with increasing spreading length. For the 10ns delay case, spreading can be easy with a high spreading length of 128. For the Pedestrian A case, to achieve the target SIR, the spreading length should be no more than 64.

For Vehicular A, the frequency spreading technique suffers from high interference that leads to low SIR. In addition, only for a high delay spread (Vehicular A), the higher the spreading length, the higher the spectral efficiency. However, a high spreading length also leads to high interference caused by the channel. Due to the high overhead needed for enough SIR, our approach is inadequate. Instead, it could be employed the multi-tap equalization at the cost of complexity.

Second, we check the validity of the described block frequency spreading approach with the benefit of restoring complex orthogonality, which is expected to enable usage of all MIMO schemes used in OFDM, for different MIMO schemes (mentioned in section II) by simulation.

The simulation parameters are the same as those in Table 3, but we take the value of the spreading length as 32 under two-channel models (Pedestrian A and Vehicular A) at 2.5 GHz. For OFDM, we use 512 subcarriers. The simulation is run with 1024 Monte Carlo repetitions. A 2 × 1 Alamouti STBC scheme, which achieves full diversity at rate one [67], is considered in Fig. 34. Figs. 35 and 36 show the performance of the FBMC 2 × 2 SM MIMO for ZF detection and ML detection, respectively. In 2 × 2 SM, independent bitstreams at both antennas are simultaneously transmitted. The transmitted symbols are detected at the receiver either by ZF equalization, which enhances the noise, or by ML detection [67], which may increase the complexity. We assume the Gaussian noise distribution and perfect knowledge of the channel. Note that ML detection in conventional FBMC is not viable because, owing to imaginary interference, too many variables have to be calculated. These figures also give a comparison of OFDM and FBMC using the proposed PFs based on WH block frequency spreading.

Figs. 34, 35 and 36 show that the frequency spreading FBMC achieves approximately the same performance as CP-OFDM for only Pedestrian A channel, but, the added benefit of higher spectral characteristics. Under Vehicular A, we observe degradation in error performance. This is because the channel induced interference which leads to an SIR of approximately 9 dB, see Fig. 33. In order to gain robustness, we might need to reduce the spreading length.

In addition, we can observe high deviations between CP-OFDM and FBMC. Due to the lack of a CP, FBMC tends to be more susceptible to long delay spread channels. CP-OFDM outperforms FBMC in the Vehicular channel. Finally, the results show that all PFs verify the validity of the WH block frequency spreading approach in FBMC with different MIMO schemes.

### 2) WALSH-HADAMARD SPREADING IN TIME

As previously explained, a coding matrix has been described that satisfies the orthogonality condition in (52) and that is based on fast WH transforms, so the additional complexity becomes very low. The main reason for spreading symbols over several time slots, as discussed in Section III, is to enable MIMO transmissions in FBMC with approximately the same MIMO complexity as in OFDM. Here, we spread in time instead of frequency. Also, we apply the same MIMO schemes described in frequency spreading and verify the validity of the block time spreading approach.

The simulation parameters are chosen as shown in Table 3, and the Pedestrian A and Vehicular A channel model is assumed. Figs. 37, 38 and 39 show that FBMC achieves approximately the same performance as CP-OFDM. However, we can observe that the higher delay spread channel (Vehicular A) cause degradation in error performance, for both CP-OFDM and FBMC, than lower delay spread channel (Pedestrian A). Additionally, all PFs verify the validity of the WH time spreading approach in FBMC with different MIMO schemes.

Compared the frequency spreading approach to the time-spreading approach, see Fig. 34 to 39, the two approaches provide approximately the same performance in time-variant channels. However, it can be seen that the CP-OFDM is more robust to long delay spread channels in the frequency spreading approach due to the presence of the CP. So far, we have presented a detailed description of how spreading can be used to restore complex orthogonality. This allows the straightforward usage of all MIMO techniques.

## V. CONCLUSION

In this work, new prototype pulse shape filters are proposed to improve the performance of FBMC/OQAM systems. The simulation results show that FBMC/OQAM provides superior spectral properties to OFDM.

The simulation results for the BER performance, under practical channel models, indicate that all proposed and conventional filters in FBMC systems achieve almost the same performance as CP-OFDM for moderate delay spread (EPA channel model). However, FBMC has better performance than CP-OFDM for high delay spread (EVA channel model). Generally, the validity of our PFs in the FBMC/OQAM system has been verified by the results in terms of the BER.

Additionally, we have studied the effects of a TO and a CFO on the SIR. Accordingly, we find that the PHYDYAS filter offers higher immunity to TO effects than the other filters, whereas Hermite is slightly better than the other filters

in the presence of a CFO. However, the simulation results for PLP (with $\alpha = 0.9$ and n=2) and LCP (with $\alpha = 0.9$ and $\gamma = 1.5$), which satisfy the Nyquist-I criterion, show an important improvement in OoB emissions reduction and thus in the time-frequency spectral efficiency with a small number of subcarriers and a small SIR between two users compared to the other proposed filters and conventional filters. Furthermore, PLP and LCP may be considered promising aspects of a new PF that can be exploited in the FBMC/OQAM system.

Additionally, we propose a new approach for MIMO FBMC/OQAM using WH spreading, which has a big advantage of low complexity. We have shown that WH spreading has almost no impact on the PSD. Additionally, we have tested the proposed spreading scheme in time and frequency with three MIMO techniques, $2 \times 1$ Alamouti STBC, $2 \times 2$ SM with ZF detection and $2 \times 2$ SM with ML detection, and compared it with CP-OFDM. The simulation results show that FBMC can obtain almost the same performance in terms of the SIR and BER as CP-OFDM. However, FBMC still outperforms OFDM because of the much better spectral properties. Furthermore, we have shown that all PFs verify the validity of the WH time and frequency spreading approach with different MIMO schemes.

## REFERENCES

[1] P. Popovski, K. F. Trillingsgaard, O. Simeone, and G. Durisi, "5G wireless network slicing for eMBB, URLLC, and mMTC: A communication-theoretic view," *IEEE Access*, vol. 6, pp. 55765–55779, 2018.

[2] S. Taheri, M. Ghoraishi, P. Xiao, and L. Zhang, "Efficient implementation of filter bank multicarrier systems using circular fast convolution," *IEEE Access*, vol. 5, pp. 2855–2869, 2017.

[3] F. Schaich and T. Wild, "Waveform contenders for 5G—OFDM vs. FBMC vs. UFMC," in *Proc. 6th Int. Symp. Commun., Control Signal Process. (ISCCSP)*, Athens, Greece, May 2014, pp. 457–460.

[4] G. Wunder. (2016). 5GNOW D1.6 v1.0 White Paper. 5GNOW. [Online]. Available: https://www.is-wireless.com/fp7-5gnow/

[5] A. F. Demir, M. H. Elkourdi, M. Ibrahim, and H. Arslan, "Waveform design for 5G and beyond," in *Proc. 5G Netw. Fundam. Requir. Enabling Technol. Oper. Manag.*, Hoboken, NJ, USA, 2018, pp. 51–76.

[6] H. K. Bizaki, *Towards 5G Wireless Networks—A Physical Layer Perspective*. Rijeka, Croatia: InTech, 2016, pp. 27–48.

[7] B. Farhang-Boroujeny and L. Lin, "Cosine modulated multitone for very high-speed digital subscriber lines," in *Proc. IEEE Int. Conf. Acoust., Speech, Signal Process. (ICASSP)*, Philadelphia, PA, USA, May 2005, pp. 345–348.

[8] G. Cherubini, E. Eleftheriou, and S. Olcer, "Filtered multitone modulation for very high-speed digital subscriber lines," *IEEE J. Sel. Areas Commun.*, vol. 20, no. 5, pp. 1016–1028, Jun. 2002.

[9] G. Cherubini, E. Eleftheriou, S. Oker, and J. M. Cioffi, "Filter bank modulation techniques for very high speed digital subscriber lines," *IEEE Commun. Mag.*, vol. 38, no. 5, pp. 98–104, May 2000.

[10] H. Myung, J. Lim, and D. Goodman, "Single carrier FDMA for uplink wireless transmission," *IEEE Veh. Technol. Mag.*, vol. 1, no. 3, pp. 30–38, Sep. 2006.

[11] G. Cherubini, E. Eleftheriou, and S. Ölçer, "Filtered multitone modulation for VDSL," in *Proc. IEEE Globecoms*, Rio de Janeireo, Brazil, Dec. 1999, pp. 1139–1144.

[12] A. Salah, H. M. Abdel-Atty, and R. Y. Rizk, "Joint channel assignment and power allocation based on maximum concurrent multicommodity flow in cognitive radio networks," *Wireless Commun. Mobile Comput.*, vol. 2018, pp. 1–14, Jul. 2018.

[13] B. Farhang-Boroujeny, "OFDM versus filter bank multicarrier," *IEEE Signal Process. Mag.*, vol. 28, no. 3, pp. 92–112, May 2011.

[14] European Project 211887 PHYDYAS. (2010). *Physical Layer for Dynamic Spectrum Access and Cognitive Radio*. [Online]. Available: http://www.ict-phydyas.org/

[15] EMPhAtiC Project. (2015). *Enhanced Multicarrier Techniques for Professional Ad-Hoc and Cell-Based Communications*. [Online]. Available: http://www.ict-emphatic.eu/

[16] 5GNOW Project. (2015). *5th Generation Non-Orthogonal Waveforms for Asynchronous Signaling (5GNOW)*. [Online]. Available: http://www.5gnow.eu/

[17] METIS Project. (2015). *Mobile and Wireless Communications Enablers for the Twenty-Twenty Information Society (METIS)*. [Online]. Available: https://www.metis2020.com/

[18] FANTASTIC 5G. (2017). *Flexible Air Interface For Scalable Service Delivery Within Wireless Communication Networks of the 5th Generation (FANTASTIC 5G)*. [Online]. Available: http://fantastic5g.eu/

[19] 5G PPP. (2018). *The 5G Infrastructure Public-Private Partnership (5G PPP)*. [Online]. Available: http://5g-ppp.eu/

[20] A. Viholainen, T. Ihalainen, T. H. Stitz, M. Renfors, and M. Bellanger, "Prototype filter design for filter bank based multicarrier transmission," in *Proc. Eur. Signal Process. Conf.*, Glasgow, U.K., 2009, pp. 1359–1363.

[21] A. Sahin, I. Guvenc, and H. Arslan, "A survey on multicarrier communications: Prototype filters, lattice structures, and implementation aspects," *IEEE Commun. Surveys Tuts.*, vol. 16, no. 3, pp. 1312–1338, 3rd Quart., 2014.

[22] A. Aminjavaheri, A. Farhang, L. E. Doyle, and B. Farhang-Boroujeny, "Prototype filter design for FBMC in massive MIMO channels," in *Proc. IEEE Int. Conf. Commun. (ICC)*, Paris, France, May 2017, pp. 1–6.

[23] J. Wen, J. Hua, F. Li, D. Wang, and J. Li, "Design of FBMC waveform by exploiting a NPR prototype filter," in *Proc. Adv. Wireless Opt. Commun. (RTUWO)*, Riga, Latvia, Nov. 2017, pp. 156–161.

[24] M. Bellanger, "FS-FBMC: An alternative scheme for filter bank based multicarrier transmission," in *Proc. 5th Int. Symp. Commun., Control Signal Process.*, Rome, Italy, May 2012, pp. 1–4.

[25] M. Schellmann, Z. Zhao, H. Lin, P. Siohan, N. Rajatheva, V. Luecken, and A. Ishaque, "FBMC-based air interface for 5G mobile: Challenges and proposed solutions," in *Proc. 9th Int. Conf. Cognit. Radio Oriented Wireless Netw.*, Oulu, Finland, 2014, pp. 102–107.

[26] M. Renfors, J. Yli-Kaakinen, and F. J. Harris, "Analysis and design of efficient and flexible fast-convolution based multirate filter banks," *IEEE Trans. Signal Process.*, vol. 62, no. 15, pp. 3768–3783, Aug. 2014.

[27] P. Siohan, C. Siclet, and N. Lacaille, "Analysis and design of OFDM/OQAM systems based on filterbank theory," *IEEE Trans. Signal Process.*, vol. 50, no. 5, pp. 1170–1183, May 2002.

[28] J. A. Zhang, X. Huang, A. Cantoni, and Y. J. Guo, "Sidelobe suppression with orthogonal projection for multicarrier systems," *IEEE Trans. Commun.*, vol. 60, no. 2, pp. 589–599, Feb. 2012.

[29] D. Chen, X.-G. Xia, T. Jiang, and X. Gao, "Properties and power spectral densities of CP based OQAM-OFDM systems," *IEEE Trans. Signal Process.*, vol. 63, no. 14, pp. 3561–3575, Jul. 2015.

[30] J.-M. Choi, Y. Oh, H. Lee, and J.-S. Seo, "Pilot-aided channel estimation utilizing intrinsic interference for FBMC/OQAM systems," *IEEE Trans. Broadcast.*, vol. 63, no. 4, pp. 644–655, Dec. 2017.

[31] Z. Jellali and L. Najjar Atallah, "Fast fading channel estimation by Kalman filtering and CIR support tracking," *IEEE Trans. Broadcast.*, vol. 63, no. 4, pp. 635–643, Dec. 2017.

[32] Y. Tian, D. Chen, K. Luo, and T. Jiang, "Prototype filter design to minimize stopband energy with constraint on channel estimation performance for OQAM/FBMC systems," *IEEE Trans. Broadcast.*, vol. 65, no. 2, pp. 260–269, Jun. 2019.

[33] V. Kumbasar and O. Kucur, "ICI reduction in OFDM systems by using improved sinc power pulse," *Digit. Signal Process.*, vol. 17, no. 6, pp. 997–1006, Nov. 2007.

[34] S. Joon Lee and N. C. Beaulieu, "Performance of the raised-cosine and 'Better than raised-Cosine' pulses in Non-Data-Aided symbol timing-error detection," in *Proc. IEEE Global Telecommun. Conf. (GLOBECOM)*, Nov. 2007, pp. 1765–1769.

[35] S. Mohanty and S. Das, "A comparative study of pulse shaping functions for ICI power reduction in OFDM system," in *Proc. Annu. IEEE India Conf.*, Kanpur, India, Dec. 2008, pp. 312–316.

[36] A. L. Onofrei and N. D. Alexandru, "The effect of ICI in OFDM systems using improved phase modified sinc pulse," in *Proc. Int. Symp. Signals, Circuits Syst.*, Iasi, Romania, Jul. 2009, pp. 1–4.

[37] S. Mirabbasi and K. Martin, "Overlapped complex-modulated transmultiplexer filters with simplified design and superior stopbands," *IEEE Trans. Circuits Syst. II. Analog Digit. Signal Process.*, vol. 50, no. 8, pp. 456–469, Aug. 2003.

[38] M. Bellanger, D. Le Ruyet, D. Roviras, M. Terré, J. Nossek, L. Baltar, Q. Bai, D. Waldhauser, M. Renfors, and T. Ihalainen, "FBMC physical layer: A primer," *Phydyas*, vol. 25, no. 4, pp. 7–10, 2010.

[39] H. Zhang, D. Le Ruyet, and M. Terre, "Spectral efficiency analysis in OFDM and OFDM/OQAM based cognitive radio networks," in *Proc. IEEE 69th Veh. Technol. Conf. (VTC Spring)*, Barcelona, Spain, Apr. 2009.

[40] S. D. Assimonis, M. Matthaiou, G. K. Karagiannidis, and J. A. Nossek, "Optimized 'better than' raised-cosine pulse for reduced ICI in OFDM systems," in *Proc. 17th Int. Conf. Telecommun.*, Doha, Qatar, Apr. 2010, pp. 249–252.

[41] D. K. Sharma, A. Mishra, and R. Saxena, "BER based performance evaluation by pulse shaping in OFDM," in *Proc. Int. Conf. Comput. Intell. Commun. Netw. (CICN)*, Bhopal, India, Nov. 2010, pp. 482–487.

[42] A. Sahin, I. Guvenc, and H. Arslan, "A comparative study of FBMC prototype filters in doubly dispersive channels," in *Proc. IEEE Globecom Workshops*, Anaheim, CA, USA, Dec. 2012, pp. 197–203.

[43] J. Du, P. Xiao, Q. Chen, and J. Wu, "Design of isotropic orthogonal transform algorithm-based multicarrier systems with blind channel estimation," *IET Commun.*, vol. 6, no. 16, pp. 2695–2704, Nov. 2012.

[44] R. Razavi, P. Xiao, and R. Tafazolli, "Information theoretic analysis of OFDM/OQAM with utilized intrinsic interference," *IEEE Signal Process. Lett.*, vol. 22, no. 5, pp. 618–622, May 2015.

[45] Y. Medjahdi, D. Le Ruyet, D. Roviras, H. Shaiek, and R. Zakaria, "On the impact of the prototype filter on FBMC sensitivity to time asynchronism," in *Proc. Int. Symp. Wireless Commun. Syst. (ISWCS)*, Paris, France, Aug. 2012, pp. 939–943.

[46] R. Saxena and H. D. Joshi, "ICI reduction in OFDM system using IMBH pulse shapes," *Wireless Pers. Commun.*, vol. 71, no. 4, pp. 2895–2911, Aug. 2013.

[47] R. Saxena and H. D. Joshi, "Performance improvement in an OFDM system with MBH combinational pulse shape," *Digit. Signal Process.*, vol. 23, no. 1, pp. 314–321, Jan. 2013.

[48] C. A. Azurdia-Meza, S. Kamal, and K. Lee, "BER enhancement of OFDM-based systems using the improved parametric linear combination pulse," in *Proc. Int. Conf. Inf. Commun. Technol. Converg. (ICTC)*, Jeju, South Korea, Oct. 2015, pp. 743–745.

[49] C. A. Azurdia-Meza, C. Estevez, A. Dehghan Firoozabadi, and I. Soto, "Evaluation of the sinc parametric linear combination pulse in digital communication systems," in *Proc. 8th IEEE Latin-Amer. Conf. Commun. (LATINCOM)*, Medellin, Colombia, Nov. 2016, pp. 1–5.

[50] H. F. Arrano and C. A. Azurdia, "ICI reduction in OFDM systems using a new family of Nyquist-I pulses," *IEEE Latin Amer. Trans.*, vol. 13, no. 11, pp. 3556–3561, Nov. 2015.

[51] C. A. Azurdia-Meza, H. F. Arraño, C. Estevez, and I. Soto, "Performance enhancement of OFDM-based systems using improved parametric linear combination pulses," *Wireless Pers. Commun.*, vol. 85, no. 3, pp. 809–824, Dec. 2015.

[52] S. Kamal, C. A. Azurdia-Meza, and K. Lee, "Family of Nyquist-I pulses to enhance orthogonal frequency division multiplexing system performance," *IETE Tech. Rev.*, vol. 33, no. 2, pp. 187–198, Mar. 2016.

[53] N. D. Alexandru and A. L. Onofrei, "ICI reduction in OFDM systems using phase modified sinc pulse," *Wireless Pers. Commun.*, vol. 53, no. 1, pp. 141–151, Mar. 2010.

[54] T. P. Fowdur and L. Doorganah, "Performance of modified and low complexity pulse shaping filters for IEEE 802.11 OFDM transmission," *J. Inf. Telecommun.*, vol. 3, no. 3, pp. 361–380, Jul. 2019.

[55] J. Aranda-Cubillo, C. A. Azurdia-Meza, S. Montejo-Sanchez, F. M. Maciel-Barboza, and I. Jiron, "Analysis of the exponential linear pulse in baseband digital communication systems," in *Proc. IEEE 9th Latin-American Conf. Commun. (LATINCOM)*, Guatemala City, Guatemala, Nov. 2017, pp. 1–6.

[56] A. Kumar and M. Magarini, "Improved nyquist pulse shaping filters for generalized frequency division multiplexing," in *Proc. 8th IEEE Latin-Amer. Conf. Commun. (LATINCOM)*, Medellin, Colombia, Nov. 2016, pp. 1–7.

[57] N. A. El-Alfi, H. M. Abdel-Atty, and M. A. Mohamed, "Cyclostationary detection of 5G GFDM waveform using time smoothing algorithms in cognitive radio transmission," in *Proc. IEEE 17th Int. Conf. Ubiquitous Wireless Broadband (ICUWB)*, Salamanca, Spain, Sep. 2017, pp. 1–6.

[58] N. A. El-Alfi, H. M. Abdel-Atty, and M. A. Mohamed, "Sub-nyquist cyclostationary detection of GFDM for wideband spectrum sensing," *IEEE Access*, vol. 7, pp. 86403–86411, 2019.

[59] T. Moazzeni, "On the compactness of OFDM and hermite signals," *IEEE Commun. Lett.*, vol. 20, no. 7, pp. 1313–1316, Apr. 2016.

[60] R. Nissel, S. Schwarz, and M. Rupp, "Filter bank multicarrier modulation schemes for future mobile communications," *IEEE J. Sel. Areas Commun.*, vol. 35, no. 8, pp. 1768–1782, Aug. 2017.

[61] A. Jayaprakash and G. R. Reddy, "Novel adaptive filter design for filter bank multicarrier system under doubly dispersive channel conditions," *IETE J. Res.*, vol. 64, no. 4, pp. 538–552, Jul. 2018.

[62] A. I. Perez-Neira, M. Caus, R. Zakaria, D. Le Ruyet, E. Kofidis, M. Haardt, X. Mestre, and Y. Cheng, "MIMO signal processing in offset-QAM based filter bank multicarrier systems," *IEEE Trans. Signal Process.*, vol. 64, no. 21, pp. 5733–5762, Nov. 2016.

[63] C. A. Faria da Rocha, B. F. Uchoa-Filho, and D. Le Ruyet, "Study of the impact of pulse shaping on the performance of spatial modulation," in *Proc. Int. Symp. Wireless Commun. Syst. (ISWCS)*, Bologna, Italy, Aug. 2017, pp. 303–307.

[64] P. Singh, H. B. Mishra, A. K. Jagannatham, K. Vasudevan, and L. Hanzo, "Uplink sum-rate and power scaling laws for multi-user massive MIMO-FBMC systems," *IEEE Trans. Commun.*, vol. 68, no. 1, pp. 161–176, Jan. 2020.

[65] M. El Tabach, J.-P. Javaudin, and M. Helard, "Spatial data multiplexing over OFDM/OQAM modulations," in *Proc. IEEE Int. Conf. Commun.*, Glasgow, U.K., Jun. 2007, pp. 4201–4206.

[66] P. Singh and K. Vasudevan, "Time domain channel estimation for MIMO-FBMC/OQAM systems," *Wireless Pers. Commun.*, vol. 108, no. 4, pp. 2159–2178, Oct. 2019.

[67] R. Zakaria and D. Le Ruyet, "A novel filter-bank multicarrier scheme to mitigate the intrinsic interference: Application to MIMO systems," *IEEE Trans. Wireless Commun.*, vol. 11, no. 3, pp. 1112–1123, Mar. 2012.

[68] P. Singh, R. Budhiraja, and K. Vasudevan, "SER analysis of MMSE combining for MIMO FBMC-OQAM systems with imperfect CSI," *IEEE Commun. Lett.*, vol. 23, no. 2, pp. 226–229, Feb. 2019.

[69] H. Lin, C. Lele, and P. Siohan, "A pseudo alamouti transceiver design for OFDM/OQAM modulation with cyclic prefix," in *Proc. IEEE 10th Workshop Signal Process. Adv. Wireless Commun.*, Perugia, Italy, Jun. 2009, pp. 300–304.

[70] C. Le and S. Moghaddamnia, "On the performance of alamouti scheme in 2 × 2 MIMO-FBMC systems," in *Proc. 19th Int. Conf. OFDM Freq. Domain Techn.*, Essen, Germany, 2016, pp. 1–6.

[71] M. Renfors, T. Ihalainen, and T. H. Stitz, "A block-alamouti scheme for filter bank based multicarrier transmission," in *Proc. Eur. Wireless Conf. (EW)*, Lucca, Italy, 2010, pp. 1031–1037.

[72] W. Raslan, M. Mohamed, and H. Abdel-Atty, "Complementary FBMC/OQAM for future Internet of Things wireless communications," presented at the 7th Japan-Africa Conf. Electron., Commun., Comput. (JAC-ECC), Alexandria, Egypt, Dec. 16, 2019.

[73] P. Singh, E. Sharma, K. Vasudevan, and R. Budhiraja, "CFO and channel estimation for frequency selective MIMO-FBMC/OQAM systems," *IEEE Wireless Commun. Lett.*, vol. 7, no. 5, pp. 844–847, Oct. 2018.

[74] P. Singh, B. U. Rani, H. B. Mishra, and K. Vasudevan, "Neighbourhood detection-based ZF-V-BLAST architecture for MIMO-FBMC-OQAM systems," in *Proc. IEEE Global Commun. Conf. (GLOBECOM)*, Dec. 2018, pp. 1–6.

[75] R. Nissel, J. Blumenstein, and M. Rupp, "Block frequency spreading: A method for low-complexity MIMO in FBMC-OQAM," in *Proc. IEEE 18th Int. Workshop Signal Process. Adv. Wireless Commun. (SPAWC)*, Sapporo, Japan, Jul. 2017.

[76] R. Nissel and M. Rupp, "Enabling low-complexity MIMO in FBMC-OQAM," in *Proc. IEEE Globecom Workshops (GC Wkshps)*, Washington, DC, USA, Dec. 2016, pp. 1–6.

[77] P. Sabeti, H. Saeedi-Sourck, and M. J. Omidi, "Low-complexity CFO correction of frequency-spreading SMT in uplink of multicarrier multiple access networks," in *Proc. 23rd Iranian Conf. Electr. Eng.*, Tehran, Iran, May 2015, pp. 410–415.

[78] P. Singh, H. B. Mishra, A. K. Jagannatham, and K. Vasudevan, "Semi-blind, training, and data-aided channel estimation schemes for MIMO-FBMC-OQAM systems," *IEEE Trans. Signal Process.*, vol. 67, no. 18, pp. 4668–4682, Sep. 2019.

[79] P. Singh, R. Budhiraja, and K. Vasudevan, "Probability of error in MMSE detection for MIMO-FBMC-OQAM systems," *IEEE Trans. Veh. Technol.*, vol. 68, no. 8, pp. 8196–8200, Aug. 2019.

[80] A. Goldsmith, *Wireless Communications*. Cambridge, U.K.: Cambridge Univ. Press, 2005.

[81] R. van Nee, A. van Zelst, and G. Awater, "Maximum likelihood decoding in a space division multiplexing system," in *Proc. IEEE 51st Veh. Technol. Conf. (VTC-Spring)*, Tokyo, Japan, May 2000, pp. 6–10.

[82] K. Gentile, "The care and feeding of digital pulse-shaping filters," *RF Des.*, vol. 25, no. 4, pp. 50–58, 2002.

[83] N. S. Alagha and P. Kabal, "Generalized raised-cosine filters," *IEEE Trans. Commun.*, vol. 47, no. 7, pp. 989–997, Jul. 1999.

[84] N. C. Beaulieu, C. C. Tan, and M. O. Damen, "A 'better than' Nyquist pulse," *IEEE Commun. Lett.*, vol. 5, no. 9, pp. 367–368, Sep. 2001.

[85] J. K. Gautam, A. Kumar, and R. Saxena, "On the modified bartlett-hanning window (family)," *IEEE Trans. Signal Process.*, vol. 44, no. 8, pp. 2098–2102, Aug. 1996.

[86] N. C. Beaulieu and M. O. Damen, "Parametric construction of Nyquist-I pulses," *IEEE Trans. Commun.*, vol. 52, no. 12, pp. 2134–2142, Dec. 2004.

[87] J. O. Scanlan, "Pulses satisfying the Nyquist criterion," *Electron. Lett.*, vol. 28, no. 1, pp. 50–52, Jan. 1992.

[88] B. Farhang-Boroujeny, "A square-root Nyquist (M) filter design for digital communication systems," *IEEE Trans. Signal Process.*, vol. 56, no. 5, pp. 2127–2132, May 2008.

[89] P. Sandeep, S. Chandan, and A. K. Chaturvedi, "ISI-free pulses with reduced sensitivity to timing errors," *IEEE Commun. Lett.*, vol. 9, no. 4, pp. 292–294, Apr. 2005.

[90] S. Mirabbasi and K. Martin, "Design of prototype filter for near-perfect-reconstruction overlapped complex-modulated transmultiplex-ers," in *Proc. IEEE Int. Symp. Circuits Systems.*, Phoenix-Scottsdale, AZ, USA, May 2002, p. 1.

[91] M. G. Bellanger, "Specification and design of a prototype filter for filter bank based multicarrier transmission," in *Proc. IEEE Int. Conf. Acoust., Speech, Signal Process.*, Salt Lake City, UT, USA, May 2001, pp. 2417–2420.

[92] R. Haas and J.-C. Belfiore, "A time-frequency well-localized pulse for multiple carrier transmission," *Wireless Pers. Commun.*, vol. 5, no. 1, pp. 1–18, Jan. 1997.

[93] T. Strohmer and H. G. Feichtinger, *Gabor Analysis and Algorithms: Theory and Applications* (Applied and Numerical Harmonic Analysis). New York, NY, USA: Springer, 2012.

[94] J. Manz, "A sequency-ordered fast Walsh transform," *IEEE Trans. Audio Electroacoust.*, vol. AU-20, no. 3, pp. 204–205, Aug. 1972.

[95] *LTE; Evolved Universal Terrestrial Radi Access (E-UTRA); Base Station (BS) Radio Transmission and Reception*, document 3GPP TS 36.104 version 12.8.0 Release 12, ETSI TS 136 104 V12.8.0 (2015-07), 2015.

[96] H. Asplund, K. Larsson, and P. Okvist, "How typical is the 'typical urban' channel model?" in *Proc. IEEE Veh. Technol. Conf. (VTC Spring)*, Singapore, May 2008, pp. 340–343.

[97] C.-H. Yih, "BER analysis of OFDM systems impaired by DC offset and carrier frequency offset in multipath fading channels," *IEEE Commun. Lett.*, vol. 11, no. 11, pp. 842–844, Nov. 2007.

[98] T. Wang, J. G. Proakis, E. Masry, and J. R. Zeidler, "Performance degradation of OFDM systems due to Doppler spreading," *IEEE Trans. Wireless Commun.*, vol. 5, no. 6, pp. 1422–1432, Jun. 2006.

[99] Y. Liu, X. Chen, Z. Zhong, B. Ai, D. Miao, Z. Zhao, J. Sun, Y. Teng, and H. Guan, "Waveform design for 5G networks: Analysis and comparison," *IEEE Access*, vol. 5, pp. 19282–19292, 2017.

[100] T. Beer, "Walsh transforms," *Amer. J. Phys.*, vol. 49, no. 5, pp. 466–472, 2005.

[101] *Guidelines for Evaluation of Radio Transmission Technologies for IMT-2000*, document Rec. ITU-R M.1225, 1997.

**HEBA M. ABDEL-ATTY** (Senior Member, IEEE) received the Ph.D. degree in electronics and communications engineering from the Faculty of Engineering, Port Said University, Egypt, in 2012. She has been working as an Associate Professor with the Electronics and Communications Engineering Department, since 2018. She is currently the Director of the Training Center, Faculty of Engineering, Port Said University. She has also been a Co-Founder and the Leader of Port-Said engineering day team, since 2009. She is also a Founder and a Counselor of IEEE in Port-Said University student branch. She has published a lot of articles in international journals and conferences. She is a reviewer at a lot of international journals. Her current research interests are in wireless communication systems, multimedia processing, cognitive radio, security of wireless networks, artificial intelligence(AI), the Internet of Things (IoT), smart cities technologies, sustainable development, and field programmable gate array. She is also a member of IoT Egypt Forum and a member of the Technical Program Committee of IEEE Global IoT Conference and other.

**WALID A. RASLAN** (Member, IEEE) was born in Port Said, Egypt, in 1986. He received the B.S. degree in electronics and communications engineering from Suez Canal University, in 2008, and the M.S. degree in communications engineering from Mansoura University, Mansoura, Egypt, in 2014. He is currently pursuing the Ph.D. degree with Port Said University. From 2010 to 2016, he was a Research Assistant with Sinai University, Sinai, Egypt. From 2016 to 2018, he was a Lecturer with Gust University, Kuwait. Since 2018, he has been a Teaching Assistant with the Communications and Computer Engineering Department, Delta University for Science and Technology, Gamsaa, Egypt. He is the author of four articles. His research interests include wireless communication systems, new mobile generation, artificial intelligence (AI), the Internet of Things (IoT), and field programmable gate array.

**ABEER T. KHALIL** received the B.Sc. and Ph.D. degrees from the Electronics and Communications Engineering Department, Faculty of Engineering, Mansoura University, in 2001 and 2013, respectively. She is currently working as an Assistant Professor with the Faculty of Engineering, Benham University. She has published more than 20 articles and supervised ten postgraduate students in many universities. She is interested in wireless networking and hardware realizations of digital systems.

● ● ●